LOAN DOCUMENT

PHOTOGRAPH THIS SHEET

AD-A237 330

DTIC ACCESSION NUMBER

LEVEL

INVENTORY

WRDC-TR-89-4122

DOCUMENT IDENTIFICATION

Dec 1989

DISTRIBUTION STATEMENT A

Approved for public release;
Distribution Unlimited

DISTRIBUTION STATEMENT

DTIC
ELECTE
S JUN 2 7 1991 D
E

DATE ACCESSIONED

DATE RETURNED

91-03189

DATE RECEIVED IN DTIC

REGISTERED OR CERTIFIED NUMBER

H
A
N
D
L
E

W
I
T
H

C
A
R
E

PHOTOGRAPH THIS SHEET AND RETURN TO DTIC-FDAC

WRDC-TR-89-4122

AD-A237 330

COMBINED HOLOGRAPHIC-
INFRARED INSPECTION
INSTRUMENTATION

E.S. Gaynor
T.S. Jones
B.E. Pietsch
H. Berger

Industrial Quality, Inc.
19634 Club House Road
P.O. Box 2519
Gaithersburg, MD 20879

December 1989

Final Report for Period August 1987 - August 1989
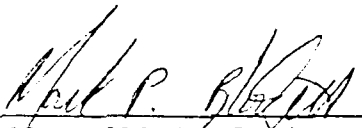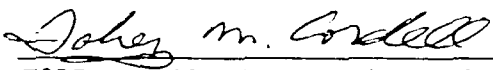
Approved for public release; distribution unlimited

NOTICE

When Government drawings, specifications, or other data are used for any purpose other than in connection with a definitely Government-related procurement, the United States Government incurs no responsibility or any obligation whatsoever. The fact that the government may have formulated or in any way supplied the said drawings, specifications, or other data, is not to be regarded by implication, or otherwise in any manner construed, as licensing the holder, or any other person or corporation; or as conveying any rights or permission to manufacture, use, or sell any patented invention that may in any way be related thereto.
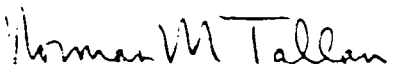
This report is releasable to the National Technical Information Service (NTIS). At NTIS, it will be available to the general public, including foreign nations.

This technical report has been reviewed and is approved for publication.

MARK BLODGETT, Project Engineer
Nondestructive Evaluation Branch
Metals and Ceramics Division
Materials Directorate

TOBEY M. CORDELL, Acting Chief
Nondestructive Evaluation Branch
Metals and Ceramics Division
Materials Directorate

FOR THE COMMANDER

NORMAN M. TALLAN, Director
Metals and Ceramics Division
Materials Directorate

If your address has changed, if you wish to be removed from our mailing list, or if the addressee is no longer employed by your organization please notify WRDC/MLLP, WPAFB, OH 45433-6533 to help us maintain a current mailing list.

Copies of this report should not be returned unless return is required by security considerations, contractual obligations, or notice on a specific document.

REPORT DOCUMENTATION PAGE

1a. REPORT SECURITY CLASSIFICATION	1b. RESTRICTIVE MARKINGS
Unclassified	

2a. SECURITY CLASSIFICATION AUTHORITY	3. DISTRIBUTION/AVAILABILITY OF REPORT
	Approved for public release; distribution unlimited.
2b. DECLASSIFICATION/DOWNGRADING SCHEDULE	

4. PERFORMING ORGANIZATION REPORT NUMBER(S)	5. MONITORING ORGANIZATION REPORT NUMBER(S)
IQI-F-89-1130	WRDC-TR-89-4122

6a. NAME OF PERFORMING ORGANIZATION	6b. OFFICE SYMBOL (If applicable)	7a. NAME OF MONITORING ORGANIZATION
Industrial Quality, Inc.		Materials Laboratory (WRDC/MLLP) Wright Research Development Center

6c. ADDRESS (City, State, and ZIP Code)	7b. ADDRESS (City, State, and ZIP Code)
19634 Club House Road, Suite 320 Gaithersburg, MD 20879	Wright-Patterson AFB, OH 45433-6533

8a. NAME OF FUNDING/SPONSORING ORGANIZATION	8b. OFFICE SYMBOL (If applicable)	9. PROCUREMENT INSTRUMENT IDENTIFICATION NUMBER
Air Force Systems Command	ASD/PMRRA	Contract No. F33615-87-C-5204

8c. ADDRESS (City, State, and ZIP Code)	10. SOURCE OF FUNDING NOS.			
Department of the Air Force ASD/PMRRA Wright-Patterson AFB, OH 45433-6503	PROGRAM ELEMENT NO.	PROJECT NO.	TASK NO.	WORK UNIT NO.
	65502F	3005	51	17

11. TITLE (Include Security Classification)
Combined Holographic-Infrared Inspection Instrumentation

12. PERSONAL AUTHOR(S)
Edwin S. Gaynor, Thomas S. Jones, Benjamin E. Pietsch, Harold Berger

13a. TYPE OF REPORT	13b. TIME COVERED	14. DATE OF REPORT (Yr., Mo., Day)	15. PAGE COUNT
Final Report	FROM 8/87 TO 8/89	1989, November, 30	75

16. SUPPLEMENTARY NOTATION
This is a Small Business Innovation Research Program, Phase II report.

17. COSATI CODES			18. SUBJECT TERMS (Continue on reverse if necessary and identify by block number)
FIELD	GROUP	SUB. GR.	Optical holography, holographic interferometry, infrared imaging, thermography, nondestructive testing, composite inspection

19. ABSTRACT (Continue on reverse if necessary and identify by block number)

An investigation of a combined holographic-infrared inspection system is reported. Thermal loading of the inspection sample yields responses from both holographic interferometry and thermographic imaging. The combined nondestructive testing approach provides additional diagnostic information, more than can be obtained from either inspection system alone. Inspection can be accomplished by real-time observation of the two images. More complete quantitative inspection information can be obtained by computer analysis of the images at various times after the thermal excitation. The inspection method is particularly useful for nondestructive testing of composite structures. Plans are being made to commercialize this SBIR development.

20. DISTRIBUTION/AVAILABILITY OF ABSTRACT	21. ABSTRACT SECURITY CLASSIFICATION
X UNCLASSIFIED/UNLIMITED ___ SAME AS RPT ___ DTIC USERS	Unclassified

22a. NAME OF RESPONSIBLE INDIVIDUAL	22b. TELEPHONE NUMBER (Include Area Code)	22c. OFFICE SYMBOL
Mark P. Blodgett	(513) 255-9805	WRDC/MLLP

DD FORM 1473, 84 MAR   83 APR edition may be used until exhausted.   Unclassified

All other editions are obsolete

EXECUTIVE SUMMARY

The objective of this Small Business Innovative Research (SBIR) program was to develop a combined dual mode nondestructive inspection system for the analysis of composite aerospace structures. The two inspection modes to be combined were infrared thermal scanning and optical holographic interferometry. The combination of these two inspection modalities offers particular attraction because both methods can be used to measure the reaction of the component to a thermal pulse stimulus; however, the two systems are sensitive to somewhat different discontinuity types. Thus the combination of the two techniques offers the opportunity to gain a greater understanding of the component condition than is provided by either inspection alone. The combined inspection system is particularly effective for use with thin composite laminates and composite skinned honeycomb assemblies.

An initial feasibility study in which the two inspection modalities were evaluated on the same components but in separate tests confirmed that both systems could be effectively used with similar thermal pulse inputs. The Phase II program provided the prototype equipment and developed the experimental technique and data analysis tools to provide maximum utility with the two systems in simultaneous operation. A high power flash tube produces useful thermal excitation of very short duration which aids in the determination of flaw depth location using time to indication information.

FOREWORD

This document reports the results of a 2-year Small Business Innovation Research (SBIR) program investigation directed toward the development of a novel dual mode inspection system for the evaluation of composite laminate and honeycomb sandwich assemblies. The effort was funded under contract F33615-87-C-5204. The approach reported involves the simultaneous imaging of the component under test using scanning infrared thermography and laser holographic interferometry.

ACKNOWLEDGEMENTS

CONTENTS

CONTENTS (Continued)

ILLUSTRATIONS

INTRODUCTION

Optical Interferometric Holography

A hologram is an interference pattern that can be used to reconstruct the optical wavefront that originally emanated (owing to reflection or transmission) from an object. The hologram is formed by the superposition of two wavefronts, an object beam and a reference beam, on a suitable recording material, such as a photographic film. When properly illuminated by the reference beam, an observer looking through the developed hologram sees a virtual image of the original object. Recording and reconstruction of a hologram are illustrated in the upper part of Figure 1.

When the real object undergoes a small displacement over part of the surface, due to stressing by thermal or mechanical means, a variation in the relative phase for the wavefronts will be produced and a fringe pattern can be observed. A real-time holographic system, as in Figure 1, permits a viewer to see the object with a fringe pattern superimposed.

If we consider a simple case in which displacement occurs in only one dimension, z, where the displacement of each point is given by the function $z = z(x)$, then by considering the change in optical path length and the wavelength, (λ) of the coherent (laser) light used to prepare and reconstruct the hologram, the Nth bright fringe corresponds to a phase change of $2\pi N = (2\pi/\lambda)[2z(x)]$. This can be simplified to show that the displacement of the surface, z(x), for the Nth bright fringe is

$$z(x) = N\lambda/2 \qquad\qquad 1)$$

In actual situations where the movement of the object surface may be due to a combination of deformation, rotation and translation simultaneously, the calculation is more complex. Nevertheless, the concept of relating fringe number and spacing to actual physical displacement is valid and can be used to obtain quantitative information from a holographic interferogram.

Holographic interferometry has been known for some time.[1-5] The technique has been used for a variety of applications shown in the review by Vest.[6] Applications have included inspections of tires, composites, honeycomb structures, bonded assemblies, ceramics, etc. to detect delaminations and bond problems, thin areas, cracks and similar discontinuities. Thermal stressing for holographic interferometry has been used in methods that have included overall temperature changes, heat lamps and flash tubes; examples of thermal stressed holographic interferometry are discussed in References 7 and 8.

The technique of holographic interferometry is reasonably well developed. Capable investigators have been able to apply the method to a range of inspection problems.[9-13] Developments have included improved methods for fringe control[14] and improved methods for processing holograms in place using better film methods and/or thermoplastic recording techniques. These latter approaches have led to useful industrial holographic equipment that can be used on the factory floor.

An example of an interferogram is shown in Figure 2. The sample is a glass epoxy tube which has suffered impact damage. The impact damaged area is clearly seen as a densification of the fringe lines with additional fringe line distortion along the sides of the damaged area.

RECORDING

Laser

Lens-Pinhole Assembly

Reference Mirror

Honeycomb Sandwich Structure (Object)

Photographic Plate

VIEWING

Laser

Lens-Pinhole Assembly

Observer or Camera

Reference Mirror

Reconstructed Virtual Image of the Object

Developed Hologram

Real-time Hologram

Flaw (Void in Adhesive)

Honeycomb Core

Skin

Adhesive
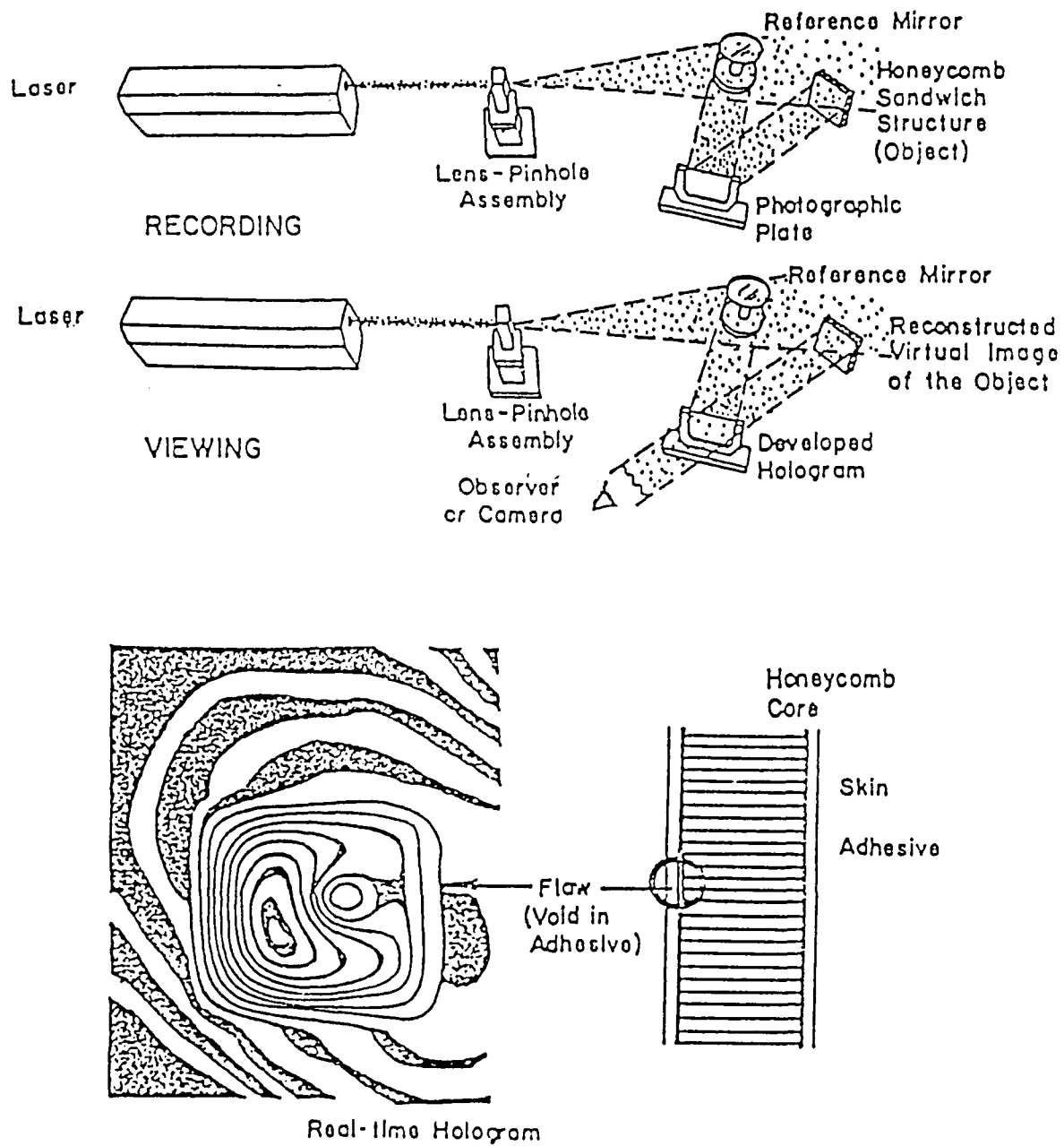
Figure 1. Real-Time Holographic Interferometry

Figure 2. Interferometric Hologram of Impact Damaged Composite Tube

Infrared Thermography

All bodies above the temperature absolute zero emit electromagnetic radiation by virtue of the motion of the constituent atoms. The spectrum and intensity of the radiation depend on the temperature and nature of the surface. When a surface is heated, there is an increase in energy of the atomic particles leading to a corresponding increase in temperature and emitted energy. The *wavelength-independent* rate of emission of radiant energy per unit area is governed by the Stefan-Boltzmann law:

$$W = \epsilon\sigma T^4 \qquad \qquad 2)$$

where

$\quad$ W = rate of emission, radiant energy per unit area
$\quad$ ϵ = emissivity (ratio of emittance of the surface relative to a black body)
$\quad$ σ = Stefan-Boltzmann constant = 5.7×10^{-8} (watts/m^2 - degrees K^4)
$\quad$ T = absolute temperature, degrees Kelvin

The emittance *in a particular differential wavelength band* is governed by the Planck distribution criterion. Important criteria for practical infrared imaging are the spectrum of the emitted energy, and in particular, the wavelength of maximum emittance. These are given by the single temperature evaluation of Planck's Law and Wien's Displacement Law, respectively. Figure 3 shows a family of such energy distribution curves. For the practical case of a body at a temperature of 300°K, the wavelength range of peak emission is in the 9-to-10 μm range. This turns out to be a very useful wavelength range. Various components of our atmosphere, notably water, absorb a great deal of the emitted infrared energy. However, there are two fairly transparent windows through the atmosphere: one between 3 - 5 μm and the other at about 8 - 14 μm. Specific infrared detector elements have been developed which respond well to each of these wavelength bands.

Infrared imaging has been well developed, particularly for military applications.[15] Thermographic methods have been used to display object temperature differences for a variety of inspection applications.[16-31] Many of the inspection systems provide a television type image display. Typical sensitivity of the instruments is 0.1 degrees C.

Combined Holographic - Infrared Inspection Approach

The combination of the two inspection modalities offers several attractive features. First, both inspection methods can be effectively activated by a thermal pulse. The impact of the thermal pulse on the surface temperature pattern (for the infrared imaging) is rather apparent. The change in temperature also produces a local deformation through thermal expansion. The differential expansion between the warmer areas and the cooler areas induces a stress pattern which can produce out-of-plane surface displacements useful in the holographic interferometry method.

Both inspection methods tend to be effective on similar sample geometries. Both are ideally suited to thin composite laminates and composite skinned honeycomb sandwich panels. The sensitivity of both methods falls off with flaw depth. The two modalities are not, however, sensitive to precisely the same flaw types. While both methods tend to be sensitive to disbonds and delaminations, infrared inspection can detect many foreign materials which, though bonded in to the laminate, produce a change in thermal conductivity. Conversely, a delamination between different layers of low thermal conductivity materials, such as a bond problem between foam-to-foam structures, is difficult to detect with infrared imaging; such a defect may be more readily detected by holographic inspection.
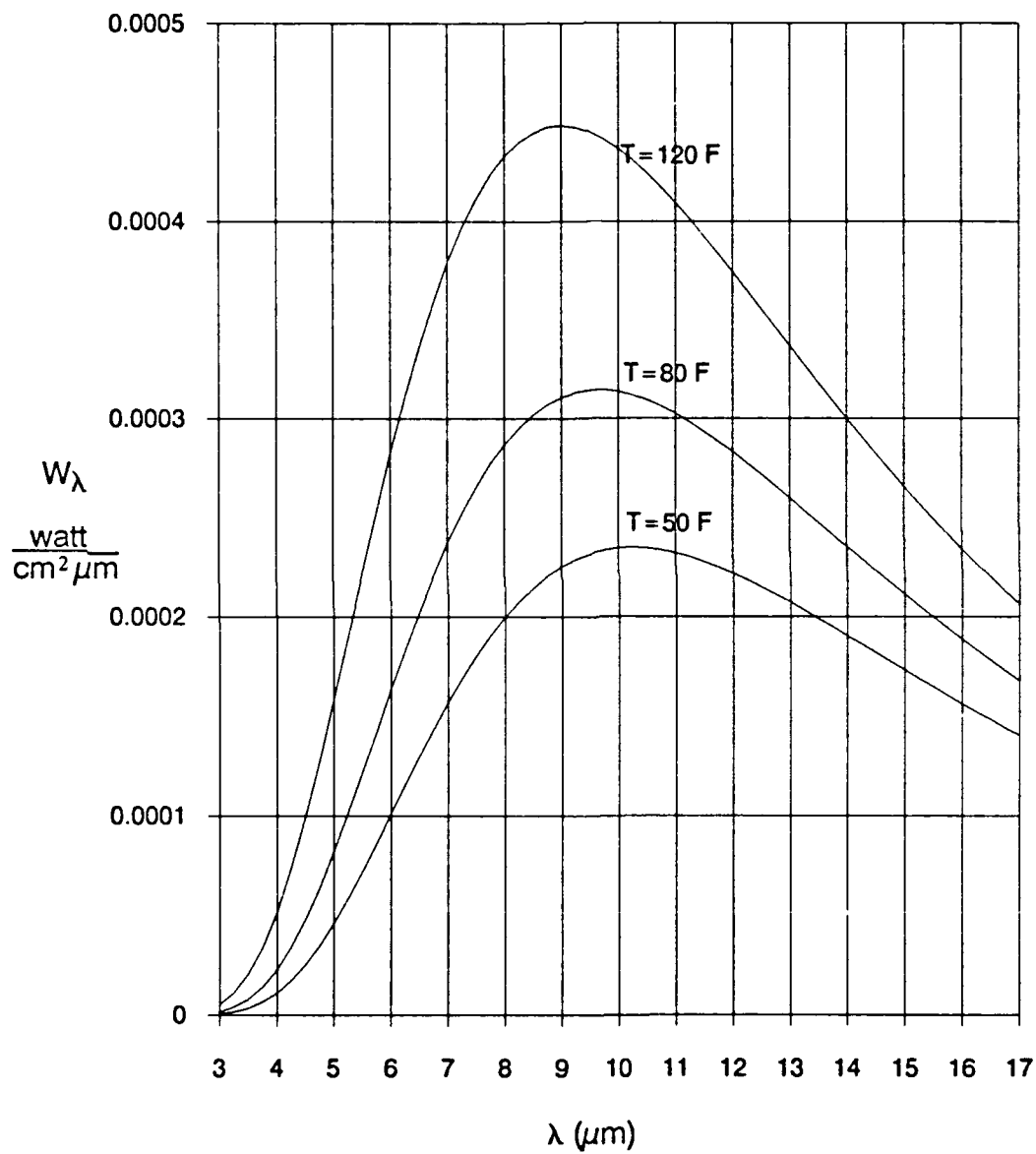
Figure 3. Spectral Radiant Emittance Distribution at Three Background Temperatures

Phase II Program Objectives

The primary objective of the Phase II program was to develop and evaluate a combined holographic-infrared inspection system to evaluate composite and bonded assemblies. This includes an evaluation of the effectiveness of the equipment and the development of techniques to optimize the effectiveness of the combined system.

THEORETICAL CONSIDERATIONS

Thermal Excitation Effects on Surface Temperature and Displacement

1. Introduction

The holographic-infrared analytical tool is characterized by its unique combination of two well-known analysis modalities: holographic surface displacement and infrared surface temperature determination. The combination of these two NDE techniques into a single instrument for inspection accomplishes a more complete description of sample defects through a more thorough specification of the strains within the sample's volume.

Determining the strains in a volume, given surface conditions, is a so-called inverse problem the solution of which is accomplished by making educated assumptions about conditions in the volume and on the surface and back-projecting the observed disturbances to their origins. As might be expected, the (underspecified) solution is not, in general, unique; therefore we must be satisfied with somewhat ambiguous flaw localization and description.

2. Data Fusion

NDE provides many excellent examples of underspecified inverse problems since, by its very nature, NDE calls for the determination of the invisible source of an observed disturbance. It is consequently desirable to develop means to aid the solutions of these problems. Improvements to the quality of inverse-problem solutions are provided by more thorough specification of the parameters comprising the problem, in particular, added boundary conditions or additional data inputs. Generally, we would like to improve specification with a "fusion" of data from multiple modalities.

The fusion of holographic (surface displacement) and infrared (surface temperature variation) data can accomplish a net improvement in the characterization of defects in materials, both homogeneous and composite. This particular combination is especially useful for the following three important reasons:

i.   Only a single form of excitation energy (heat impulse) is required for both holo- and IR systems.

ii.   In the combined system, a minimum of variables is added since the distributions of temperature and displacement are mutually dependent.

iii.   Temporal correlation of the two data sets (images) yields additional information not available in steady-state measurements with both modalities, i.e., the achievable specification degree is more than doubled.

3. Theory

Within the timescale of a typical measurement, equilibrium mechanical (stress and strain) conditions within the sample apply, and the following expressions describe displacements $u(x, y, z)$, $v(x, y, z)$, and $w(x, y, z)$ of an infinitesimal volume element within the sample. These equilibrium expressions, incidentally, form the basis of any materials analysis, one example of which is the description of material-supported ultrasonic waves. In the discussion to follow, the coordinate systems of the displacements (u, v, w), and the material itself (x, y, z) coincide.

$$(\lambda+G)\partial e/\partial x + G\nabla^2 u - \alpha E/(1-2\nu)\partial T/\partial x = 0 \qquad 3a)$$

$$(\lambda+G)\partial e/\partial y + G\nabla^2 v - \alpha E/(1-2\nu)\partial T/\partial y = 0 \qquad 3b)$$

$$(\lambda+G)\partial e/\partial z + G\nabla^2 w - \alpha E/(1-2\nu)\partial T/\partial z = 0 \qquad 3c)$$

In Equations 3, $e = \epsilon_x + \epsilon_y + \epsilon_z = \partial u/\partial x + \partial v/\partial y + \partial w/\partial z$; the normal strains. So

$$\partial e/\partial x = \partial^2 u/\partial x^2 + \partial^2 v/\partial x\partial y + \partial^2 w/\partial x\partial z, \qquad 4)$$

etc. And

$$\nabla^2 u = \partial^2 u/\partial x^2 + \partial^2 u/\partial y^2 + \partial^2 u/\partial z^2, \qquad 5)$$

etc. T is the temperature and λ, G, α and ν are material constants. Equations 3 describe the general distribution of normal strains, ϵ at a point (x, y, z) in a volume of material in which there exists a temperature distribution $T(x, y, z)$. The values u, v, and w are the magnitudes of the displacements of a differential volume element within the material. In our case, u is a displacement in the x direction, etc. For a surface oriented in the x-y plane, the surface displacement, w, will be in the z direction.

If the three Equations 3 are expanded, it quickly becomes apparent that this system is underspecified. Indeed, there are 3 equations and 18 unknowns. Therefore, boundary conditions (BCs) are imposed; i.e., $T(x, -a, z) = T(x, a, z) = T_1$, for constant temperature edges, etc. Several BCs of this type can contribute to the specification. Furthermore, the heat diffusion equation,

$$\partial T/\partial t = \kappa \nabla^2 T, \qquad 6)$$

can be used to make Equation 3 time dependent, with accompanying further specification. Here κ represents the material's thermal parameters, $(\kappa = K/(\sigma\rho)$, for thermal conductivity K, specific heat σ and density ρ,) and t is time.

With infrared (IR) measurement alone, surface measurements will yield $\partial T/\partial x$, and $\partial T/\partial y$. A finite element analysis will yield approximations to $\partial^2 T/\partial x^2$, $\partial^2 T/\partial y^2$, and some assumptions can be made to obtain $\partial^2 T/\partial z^2$. So most of the surface temperature information and some information about the temperature distribution with depth is available. Is this enough, together with the BCs to determine the strain distribution? It should be apparent that the answer is no, especially in view of the fact that surface shear strains, hidden in the various cross-derivatives of u, v, and w are not predeterminable by BCs. It will be necessary, therefore, to estimate these *and* surface displacement magnitudes if any information about the volume is to be gained from the surface temperature alone.

7

With holographic measurements alone, surface displacement and excitation information is all that is available. Clearly, many parameters are missing from those necessary for a full specification of the inverse problem.

With the holographic-infrared (Holo/IR) combination system, Equations 3 can be solved more explicitly, since surface displacement information is available and therefore no displacement assumption is necessary. Thus w, $\partial w/\partial z$, $\partial^2 w/\partial z^2$, $\partial^2 w/\partial x \partial z$, $\partial^2 w/\partial y \partial z$ and $\partial^2 w/\partial x \partial y$ should all be available, albeit through finite element approximation. Now, only the shear strains at the surface remain unspecified in the problem and they can therefore be obtained, assuming full knowledge of the (spatially varying in composites) material parameters. With these shear strains, some extrapolation to volume properties can be made, upon which the inverse problem of thoroughly characterizing the strains within the sample's volume apparently becomes nearly solvable.

Image Processor Overview

1. Introduction

The combination of holographic (Holo) and an infrared (IR) defect detection modalities into a comprehensive Nondestructive Evaluation (NDE) system is intuitively appealing as an improvement over that composed of either technique alone. For the concept to be defined beyond its intuitive appeal, however, it is necessary that it be specifically characterized in terms of both its capabilities and its implementation. Accordingly

i.   It is crucial to determine exactly what aspects of the combination should be exploited to arrive at a detection capability which is greater than the sum of its two parts. For example, similarities and contrasts between the Holo- and IR images will, in many cases, yield important new information.

ii.   It is necessary to determine the most effective framework within which the combination approach demonstrates its advantages. This framework should allow us to preserve the general approach of developing a technique (rather than a particular NDE solution), while still affording the important feature of demonstrability through experimentation.

An appropriate solution encompassing both of these descriptions can be found in *image processing*. The use of various image processing techniques will completely satisfy situation i above while providing the basis for situation ii.

2. Time-Space Correlation for Defect Depth Measurement

We have identified time-space correlation as the technique for obtaining information about the depth of particular material features-namely defects. Time-space correlation refers, in this case, to cross-correlations over particular corresponding areas in the two images at different times.

Each modality is demonstrably capable of yielding defect position within a depth plane; however, depth position as provided by either modality alone is ambiguously linked to defect size in the general case. Unambiguous depth position *is*, however, available in the Holo-IR system, in large part since the evolutions of the two images are temporally dissimilar.

8

In particular, the *thermal image* of the surface is a time-dependent result of heat diffusion, governed by the heat diffusion equation

$$\partial T/\partial t = \kappa \nabla^2 T.$$ (7)

Here κ represents the material's thermal parameters, ($\kappa = K/(\sigma\rho)$, for thermal conductivity, K, specific heat σ, and density, ρ), t is time, and

$$\nabla^2 = \partial^2/\partial x^2 + \partial^2/\partial y^2 + \partial^2/\partial z^2.$$ (8)

At the defect, κ will in general change its value. In this case, and according to Equation 7, first a temperature distribution anomaly occurs near the defect and then the disturbance transmits to the surface. Significantly, both of these processes take time.

On the other hand, *mechanical strains* caused by temperature gradients from the presence of defects within the sample's depth will immediately manifest themselves on the surface. To see this, consider the equilibrium strain-temperature relationship. In the x-dimension we have

$$(\lambda+G)\partial e/\partial x + G\nabla^2 u - \alpha E/(1-2\nu)\partial T/\partial x = 0$$ (9)

for

$$e = \epsilon_x + \epsilon_y + \epsilon_z = \partial u/\partial x + \partial v/\partial y + \partial w/\partial z$$ (10)

for material displacements u, v, w, and for material constants λ, G, α, and ν. Note here that a strain distribution will appear as an immediate result of a temperature gradient. Of course, we expect the evolution of the strain field to be time-dependent since the temperature distribution is. However, in the interpretation of Equation 9, there is no time lapse between the forming of the temperature distribution at the defect and a strain distribution at the surface.

In consideration of Equations 7 and 9 then, we expect that the application of a heat pulse will result in a holographic signal which immediately follows the time history of the temperature-induced strains, and a thermal signal which represents the temperature anomaly at the defect site through the diffusion history of the pulse including its interaction with the defect.

Time-space correlation therefore refers to comparisons between the two imaging modalities by finding how corresponding image pixels correlate at various times after an initial heat pulse is applied to the system. In effect then, we propose to perform a time-space correlation described mathematically as

$$R(x',y',t') = \iiint H(x,y,t) \, IR(x-x',y-y',t-t') \, dxdydt.$$ (11)

In Equation 11, the primed variables represent the position or time shift location at which the correlation is desired. The integration is carried out over the nonprimed variables, representing the areas or time periods over which the correlation is carried out. In general, we will be correlating over areas where temperature and height anomalies occur, i.e., over the defect. We expect then, that correlation peaks will occur at the centers of these areas ($x'=y'=0$), and their time-varying ($t'\neq0$) heights will correspond to changes in their relative shapes.

Other correlations may also yield important information. For example, any spatial derivative of the images could be temporally correlated. We could also spatially correlate time derivatives of each function.

In a broad sense we have performed these correlations, and they exist as processing options in the operation of the Holo/IR workstation. Actual correlations such as specifically described in Equation 11, although part of the initial data analysis concept, have remained beyond our processing capabilities. The Holo/IR product has as a major feature avoidance of the rigorous manipulations of data which would be required to arrive at exact correlations. The result is accordingly both streamlined in its presentation and faithful in its originality.

As part of the effort of realizing strict time-space correlations, much work was directed towards creating compatible displays. Work with the Surfer software [Golden Software, Golden, CO], (described below in *Experimental Accomplishments*) will be recognized as representing the bulk of this effort. Although this Surfer output is not now envisioned for the Holo/IR product, the ideas contained in its justification form a basis for the general image processing reasoning, and therefore they are presented below.

2.1 Compatibility Considerations-Linearity Among Display Parameters

Interferogram

For complete compatibility, the holographic interferogram must be encoded into a two-dimensional intensity map of the surface height variation.

Once this processing step is complete, additional preprocessing may be necessary. For example, it may be necessary that the output image dependencies be linear, i.e., that the holographic output intensity variation is proportional to height variation, and the IR output intensity variation is proportional to temperature variation. At the outset, we can see that this is true for the holographic display, but not strictly true for the IR display. A brief analysis explaining this point follows.

The holographically-produced display yields height variations along the surface (y-z) plane. For height distribution $u(y,z)$, the periodicity of fringes in the interferogram is proportional to $\partial u/\partial y$ and $\partial u/\partial z$. The Surfer fringe counting process detects fringe periodicity in the y and z directions at each surface point and directly encodes this as intensity in the final image on the CRT.

Since we will be a comparing this intensity distribution and that in the thermogram, it will be important that $\partial u/\partial y$ and $\partial u/\partial z$ are themselves directly related to the temperature distribution-at least in the case of a defect-free sample (deviations from a direct relationship may be one indication of defect presence). Thermally induced normal strains in the sample are expressed as

$$\epsilon = \partial u(x,y,z)/\partial x = \alpha T(x), \qquad\qquad 12)$$

with u, the normal (x-directed) surface displacement, a, a material constant, and $T(x)$, the temperature distribution throughout the sample's thickness. The holographic interferometry technique senses the derivative of u along the surface. In the y direction ,

$$\partial u/\partial y = \alpha \int \partial T(x,y,z)/\partial y \, dx. \qquad\qquad 13)$$

10

And in the z direction,

$$\partial u/\partial z = \alpha \int \partial T(x,y,z)/\partial z \, dx. \qquad 14)$$

Equations 13 and 14 express the interferometrically-observable surface displacement distributions at any y, z point as the integrated temperature-induced x-directed normal strains at that point. By the principle of strain superposition and assuming small displacements, this distribution is now linearly added to that caused by all other normal strains. In general, therefore, intensity variations in the holographic image will be linearly related to the normally integrated normal strain distribution, which is, in turn, linearly related to the normally integrated temperature distribution.

Thermogram

The thermal (IR) image is directly related to the infrared irradiance in watts/cm^2 which falls onto a detector array inside the IR imaging device. This irradiance is directly related to the radiance $W(\lambda,T,y,z)$ (watts/cm^2-sr) of the scene by integration through the solid angle (sr) which the imaging system subtends. W is a complicated function of λ and T.

$$W(\lambda,T)= a/(\lambda^5(e^{b/kT}-1)), \qquad 15)$$

where a and b are constants, k is Boltzman's constant, and λ is the IR wavelength.

The thermogram actually displays radiance *differences*, since

i.   The detector integrates over IR wavelength, λ, and

ii.   the image processing routine built into the IR viewer effectively subtracts a baseline radiance from the scene.

Therefore, the output image is described as the derivative:

$$\partial W/\partial T \simeq \Delta W/\Delta T \simeq W(d/T^2), \qquad 16)$$

where the approximation arises from the assumption that the IR energy (hc/λ) is much greater than the thermal energy (kT). (d is a constant, h is Planck's constant, c is the light velocity.)

To make a compatibility argument, we must consider the temperature variation along the surface, i.e.,

$$\Delta T/\Delta z \simeq \partial T/\partial z = \partial W/\partial z /(\partial W/\partial T) \simeq \partial W/\partial z \, (T^2/Wd). \qquad 17)$$

Equation 17 indicates a nonlinear relationship between surface temperature variation and the measured radiance intensity. What this means is that absolute temperature and radiance must be assumed to be constant across the extended surface of the sample. In the case of uneven illumination intensity, for example, the assumption may not be valid. This will require a calibration step in the analysis to account for variations in $\partial W/\partial z$ across the surface.

The compatibility of the two displays thus reduces to an assumption of illumination homogeneity linearity, or compensation thereof. Again, for precision quantitative comparisons of the Holo and IR images, this would be a requirement. Much of our image processing effort accordingly delivers illumination homogeneity information. During the course of

this quantification, however, we found that much use can be made of the Holo/IR combination in a *qualitative* sense, and that, in fact, the workstation is useful for defect detection and characterization from this standpoint. We remember, however, that the quantitative justifications are still valid, and it is essential to understand them for meaningful interpretation of the data. Nevertheless, calculating the effects and displaying them on the workstation screen is not now a priority goal. In this way, the Holo/IR system becomes workable "at a glance."

Thermomechanical Response of Honeycomb Panels

The thermal and mechanical responses of a laminated honeycomb structure to the application of a broad area heating source are determined in large part by the thermal effusivity of the several layers comprising the structure. Thermal effusivity is the square root of the product of thermal conductivity, material density and specific heat. The temperature at the surface and throughout the laminated structure can be predicted by knowing the values for each of these thermal properties for each layer in the structure. The effusivity values for each layer combine to determine the rate at which heat is conducted from the surface. The thermal and mechanical effects of defects, such as skin delaminations, skin-to-core disbonds, extra adhesive, and crushed core, may be predicted in each case by assuming the local insertion of an additional layer in the structure with an effusivity value higher or lower than the adjacent layers, depending upon the type of defect. Once the temperature distribution between layers is established, the mechanical behavior of the material may be predicted based upon the relative coefficients of thermal expansion and mechanical constraint on each layer.

1. Skin Delaminations

A delamination between plies of the graphite epoxy skin on the F/A-18 honeycomb panels (see panel description in *Test Panel Designs* section) was produced in test specimens by placing 3-mil nonporous Teflon coated glass fabric three plies below the surface. In fact, naturally occurring delaminations may result in a void between adjacent plies. In either case, from a thermal point of view, an additional low effusivity layer is inserted between layers of comparatively higher effusivity. Following illumination by a broad beam heating source, we would anticipate that the surface temperature surrounding the regions immediately above the skin delamination would cool more rapidly than the surface over the defect region since the heat flow through the defect is interrupted by a low effusivity layer (the defect itself). Consequently, infrared imaging of the surface is likely to show slightly higher temperatures over the regions where skin defects occur. Depending upon the total temperature difference above and below the defect zone, the lateral extent of the defect, and the stiffness of the material above the defect, the temperature difference above and below the delamination may be sufficient to cause a local buckling or bulging of the surface layers above the delamination. This out-of-plane surface displacement should be detectable using holographic interferometry. Both the temperature difference and resulting surface displacement are transient effects which disappear as the material reaches thermal equilibrium.

2. Skin-to-Core Disbonds and Crushed Core Defects

We would expect the holographic and infrared sensitivities to the detection of these defects to be similar since the net result of either is to produce thermal and mechanical discontinuities between the graphite epoxy skin and aluminum honeycomb core. In the test specimens, skin-to-core disbonds were produced using 6-mil Teflon coated glass fabric between the adhesive and the core. Crushed core results in a void being present between the core and skin adhesive. Assuming that both of these defects extend over a large number

of honeycomb cells, the thermal analysis is similar to that presented above in that a low effusivity layer is imposed between the skin and core of the layered structure. Again, we would anticipate that the local skin temperature above the defect would remain higher for a longer time than the areas surrounding it since the heat conduction path is significantly altered. Once again, infrared mapping should indicate elevated surface temperatures over the defect regions while holographic methods should detect buckling of the skin over the disbonded regions. Owing to the relative increase in depth beneath the surface, we would expect that skin-to-core disbond and crushed core defects would need to exist with larger lateral extent to permit similar detectability by either the infrared or holographic methods.

3. Excess Adhesive

Analysis of the thermal/mechanical behavior response of the sample surface near regions where an extra layer of foaming adhesive exists between the skin and honeycomb may not be as straightforward as for the previous cases. First of all, it is assumed that a strong thermal and mechanical bond exists between the adhesive and the skin and between the adhesive and the honeycomb core. Unlike the cases above where Teflon inserts may compromise the integrity of the mechanical bond, the strong adhesive bond in this case may constrain the skin of the structure from buckling or bulging in response to temperature differentials. However, the thermal "mass" of the additional adhesive, now in continuous contact with the surface skin, may provide a high effusivity relative to the normal intermittent contact of the graphite epoxy skin to the honeycomb core structure. This would tend to be particularly true of the foaming adhesive, since it contains a high percentage of metallic powder. This could then provide a heat sink which would allow heat to be conducted more quickly away from the surface. Therefore, the surface temperatures in regions immediately above excess adhesive defects may be cooler than surrounding temperatures. The rigid mechanical bonding associated with an adhesive defect, leads us to suspect that holographic methods may be less sensitive than thermographic techniques to such defects.

Finite Element Modelling of the Thermal Problem

A computer aided finite element model was begun to illustrate how heat flows through the skin of a honeycomb panel. This effort is intended solely to demonstrate an approach which could be used to more thoroughly model the problem.

Figures 4 and 5 depict the results of this preliminary modelling. The top picture in each figure shows the material composition of the elements by number and shading, the node numbers on the corners of each element, and the thermal loading condition by arrows. The lighter elements, labeled #1, are given thermal conductivity similar to graphite epoxy. Five columns of these elements depict the five layer graphite epoxy composite skin of a honeycomb sample. To the right are five columns of darker shaded elements, labeled #3, which represent the room air between the sample and inspection equipment. Buried within the graphite epoxy elements are four dark elements representing a skin delamination.

The bottom picture in each figure shows the computer calculated temperature distribution through the model. Since the model is being heated along the left surface, the hottest region is quite logically to the left. Temperature gradients, represented by a range of shades, show how heat flows especially around the defect.

In Figure 4, although the defect causes a significant disturbance of heat flow near the flaw, the air gap might not be detectable at the right surface of the composite skin. Clearly, the constant temperature across the outer surface may avoid detection by an infrared system. Holography, on the other hand, may be useful in the detection of minute surface displacements caused by such deep flaws.
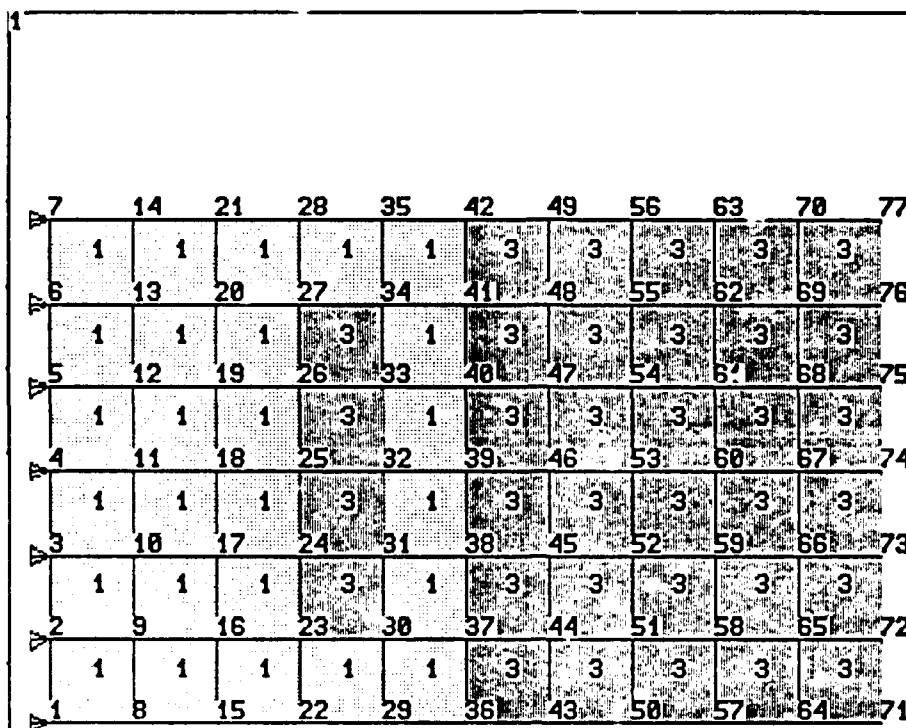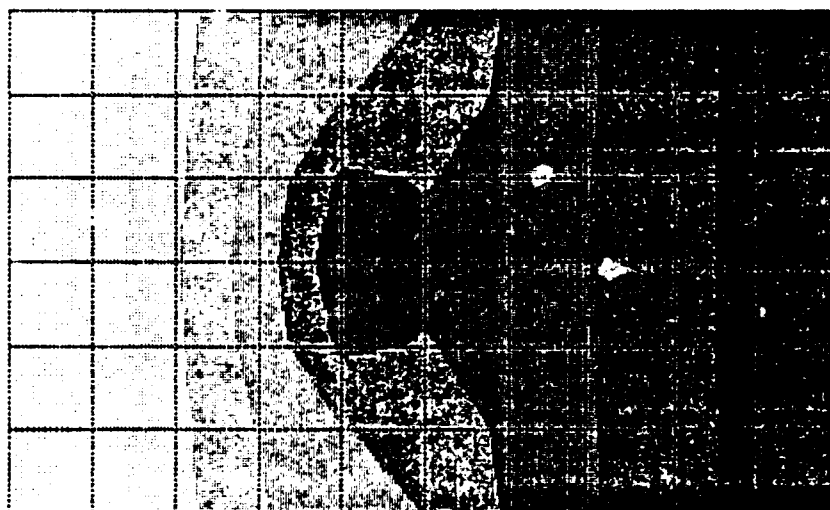
Figure 4. Finite Elements and Thermal Gradients in a Thin Graphite Epoxy Skin with Defect Far from Surface
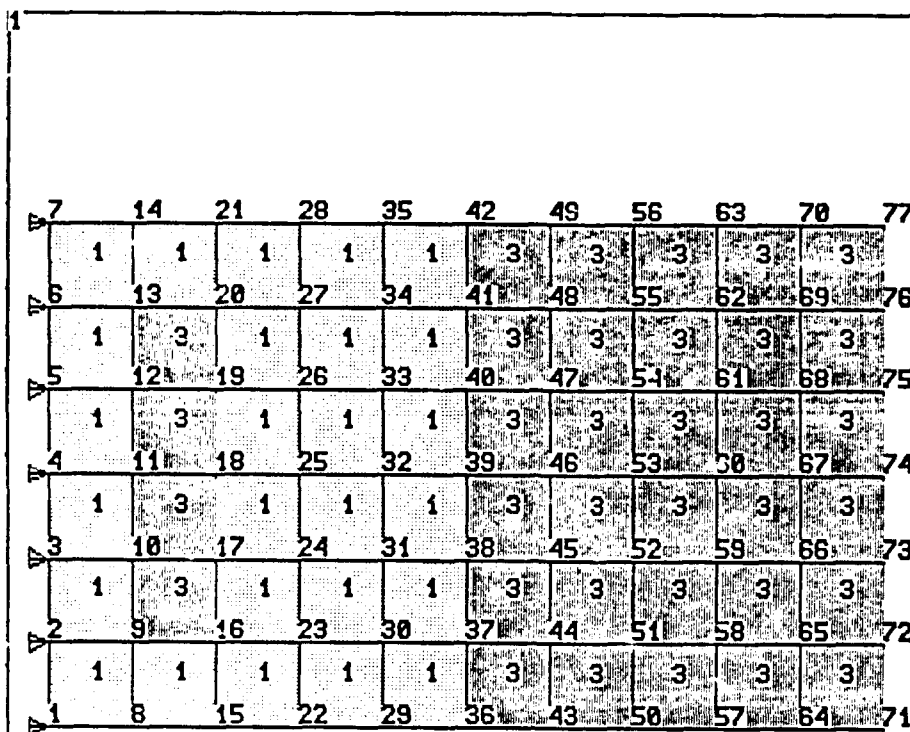
14
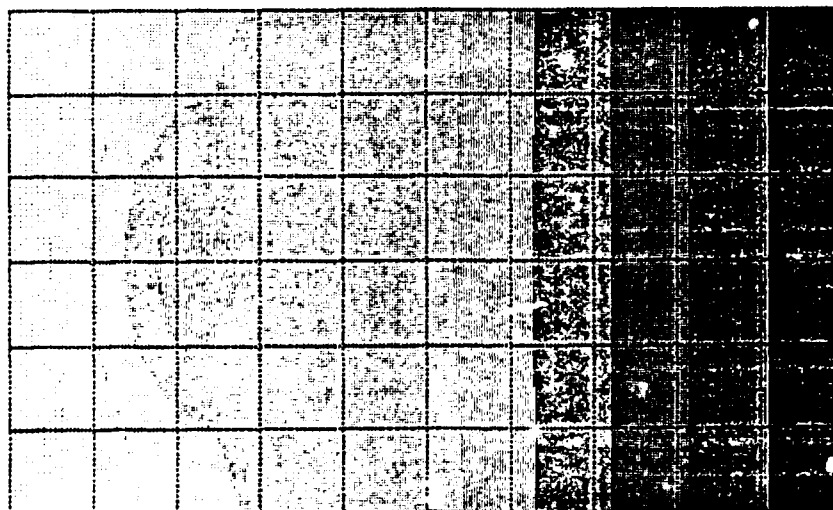
Figure 5. Finite Elements and Thermal Gradients in a Thin Graphite Epoxy Skin with Defect Close to Surface

In Figure 5, the four elements representing the air gap are closer to the surface than in Figure 4. Now the disturbance in heat flow created by the air gap casts a clear temperature differential on the right surface of the composite skin. This flaw is easily detectable by infrared.

Computer aided finite element modeling illustrates how heat flows through a thin composite laminate. From this theoretical basis, a strong case is made for inspection redundancy provided by the combined Holography/Infrared system.

Thermal Diffusion Analysis

In addition to the static heat diffusion modelling examples above, we have generated time dependent but space independent heat diffusion analyses as well in order to study the contribution of timing data to the analysis of flaw indications. The use of the short pulse excitation provided by the xenon strobe permits close empirical analysis of the time between flash excitation and image detection. By analysis of the thermal diffusion problem, we can characterize the relationship between flaw depth, time to peak indication, and material properties.

A three-dimensional finite difference solution to the thermal conduction problem was coded in FORTRAN and compiled with Microsoft FORTRAN 4.01 to run on an 80286 desktop computer. One simplifying assumption used in this analysis was to ignore in-plane variations in material conductivity. This does not mean that the significantly higher thermal conductivity in the direction of the fibers was not considered, however, since most of the laminates in which we are interested use a variety of ply orientations. The in-plane conduction through the thickness was considered to be relatively balanced. Further, since the effect we wish to model is the time required for the thermal front to travel to the defect and back to the surface, the in-plane variations have limited influence on our measurement. With this simplification, the laminate can be considered to have two independent conductivity constants, namely the in-plane conductivity and the thickness conductivity.

Analyses were carried out for a 0.400-inch-thick graphite epoxy laminate. This was chosen to be representative of the graphite epoxy flat bottomed hole (FBH) sample. The laminate was assumed to have a fiber volume fraction of 0.65. The rule of mixtures was used to determine the lamina thermal properties. Table 1 shows the influence of the fiber volume fraction on these properties. The thermal conductivity in the thickness direction was taken to be equal to the transverse conductivity given in Table 1 ($K_{zz} = 5.02$ Btu in/hr/ft^2/F). The in-plane conductivity was taken to be the average of the longitudinal and transverse conductivities ($K_{xx} = K_{yy} = (377+5.02)/2 = 191$ Btu in/hr/ft^2/F).

The analysis program was written to output the thermal contrast (temperature difference) between a point directly over a 0.5 x 0.5 inch delamination versus a point away from the flaw. This procedure was repeated for a variety of flaw depths. The results of these analyses are shown graphically in Figures 6 and 7. These figures show the calculated thermal contrast (in deg. C) as a function of time for the various flaw depths.

Figure 8 shows the relationship between the flaw depth and the time to peak indication as determined by the data used to draw the curves in Figures 6 and 7. The particular flaw depths and dimensions were selected to model several of the flat bottomed hole defects in a graphite epoxy laminate. The numbers listed next to the holes are the depths from the unmachined surface to the "top" of the hole.

The curves in Figures 6, 7, and 8 are based on an assumption that the heat pulse instantaneously raises the surface temperature 20°C. The actual value of this number is not

16

Table 1. Lamina Thermal Properties for Graphite Epoxy

Type of Fiber	Carbon
Type of Matrix	Epoxy
Fiber Density (lb/in^3)	0.065
Matrix Density (lb/in^3)	0.045
Fiber Heat Capacity (Btu/lb/°F)	0.20
Matrix Heat Capacity (Btu/lb/°F)	0.25
Fiber Long. Conductivity (Btu in/hr/ft^2/°F)	580
Fiber Trans. Conductivity (Btu in/hr/ft^2/°F)	58
Matrix Conductivity (Btu in/hr/ft^2/°F)	1.25

Fiber Volume Percent	30%	35%	40%	45%	50%	55%	60%	65%	70%	75%	80%
Lamina Heat Capacity	0.231	0.228	0.225	0.223	0.220	0.218	0.216	0.214	0.211	0.209	0.207
Longitudinal Conductivity	175	204	233	262	291	320	349	377	406	435	464
Transverse Conductivity	2.04	2.27	2.53	2.85	3.23	3.70	4.28	5.02	5.97	7.26	9.09
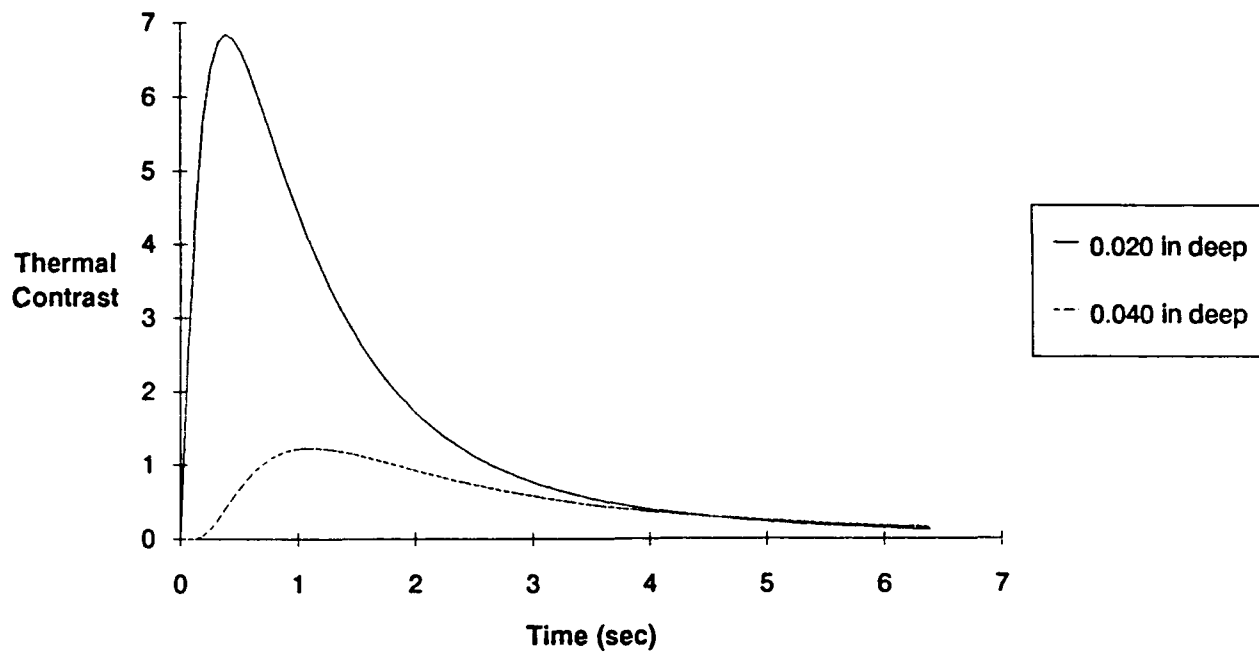
Figure 6. Thermal Contrasts for Shallow Delaminations
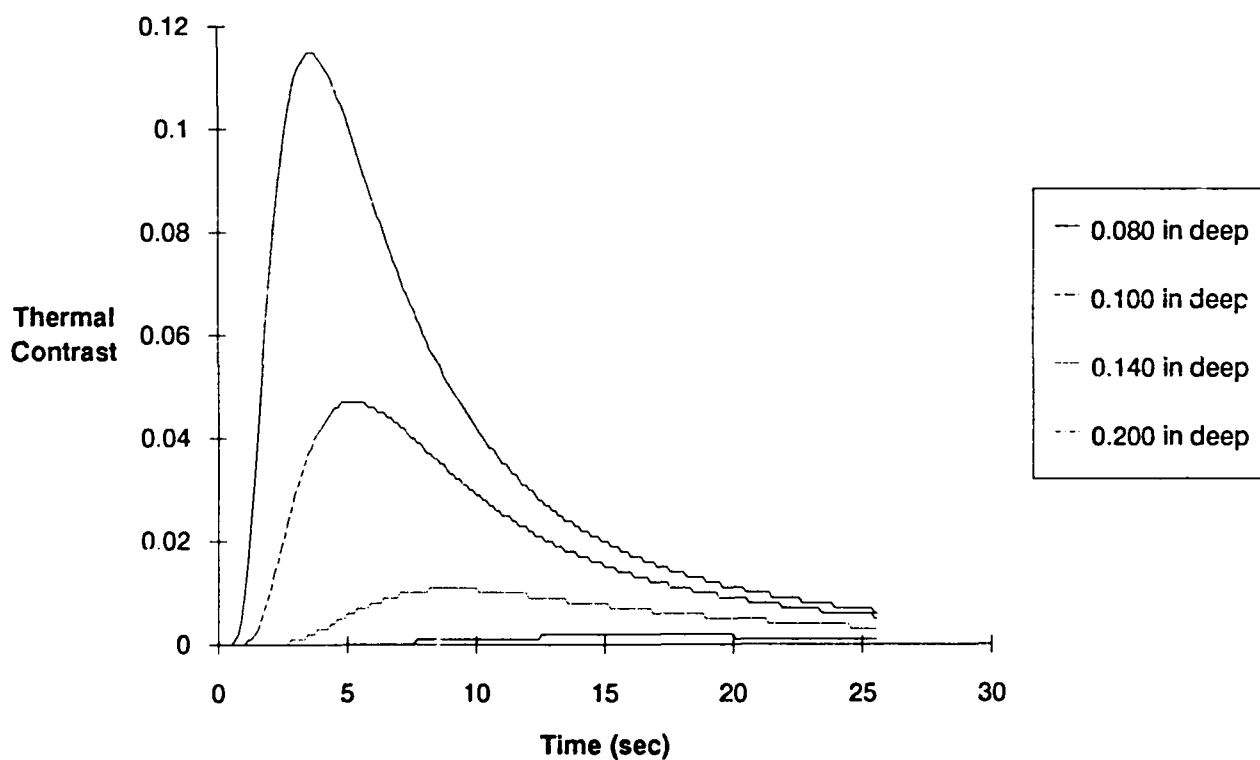
Figure 7. Thermal Contrasts for Deeper Delaminations
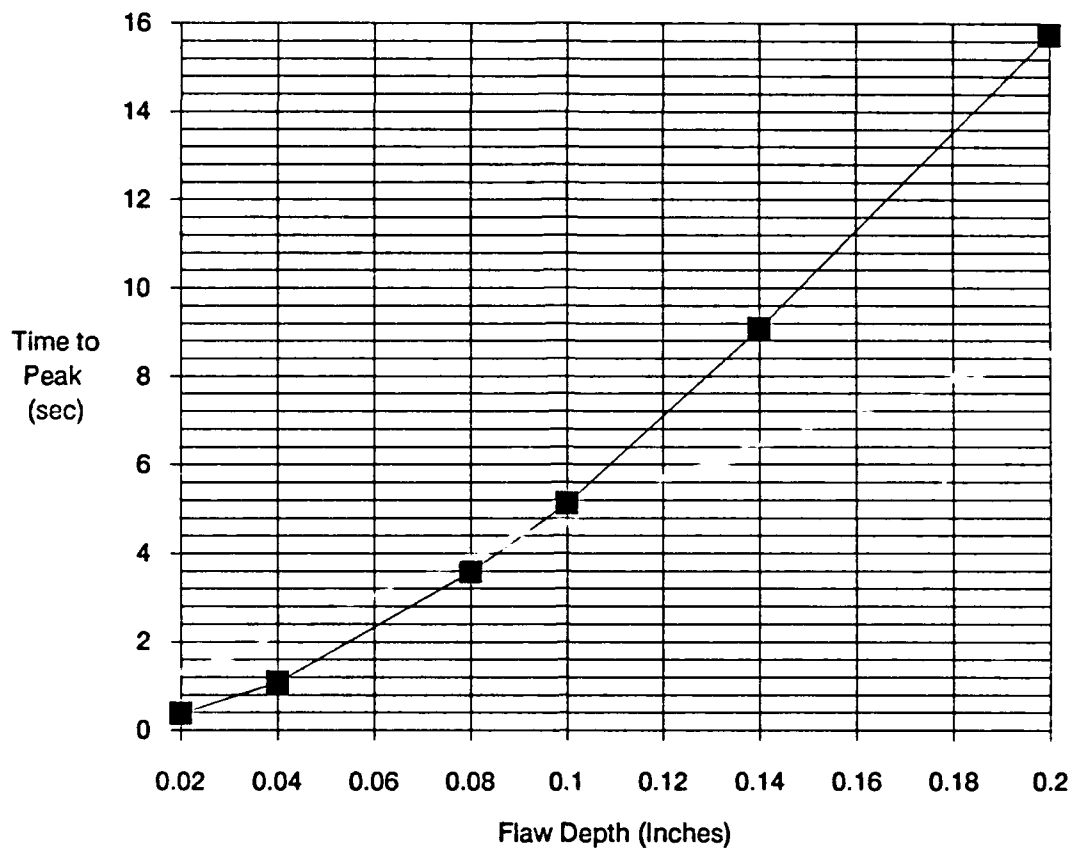
Figure 8. Time to Peak Contrast vs. Flaw Depth
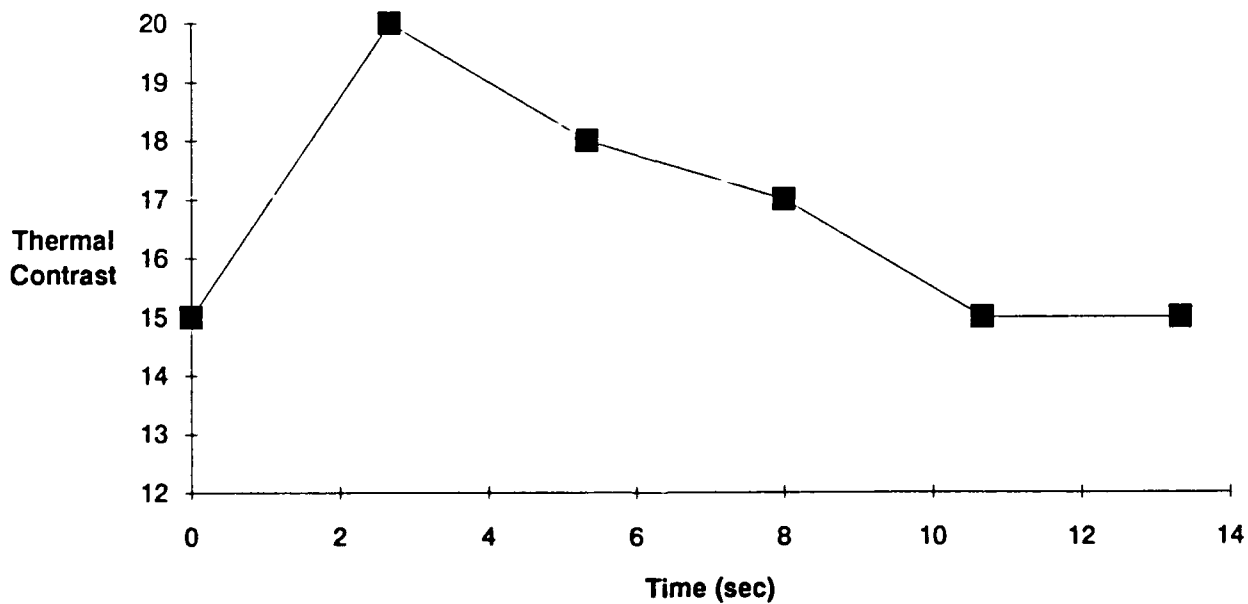
Figure 9. Experimental Result for 0.013-in-Deep Flaw

terribly important since it represents essentially a scale factor. Thus the absolute value of the thermal contrasts is not significant, however, the relationship between the curves is.

Figure 9 presents experimental results of thermal diffusion in the FBH sample for the shallowest hole. (0.013 in.) The scale is again arbitrary, but note that the shape is similar to the calculated curve. The timing does not correlate precisely. This may be due to the material composition being incorrectly modeled. It is likely that a minor change will bring the curves into coincidence.

A more empirical approach to flaw depth determination involves the use of a known standard. The sample shown schematically in Figure 10a contains 1-mil Grafoil inserts at 4, 8, 12, and 16-ply depths in a 16-ply laminate skin bonded to nonmetallic core material. The sample is shown thermally in Figure 10b following the introduction of a known amount of heat. The point intensity function of the IR scanner can be used to determine the resulting temperature at each flaw location. A plot of pixel intensity versus flaw depth is shown in Figure 11.

EQUIPMENT AND OPERATION

Selection/Description of Components

1. Infrared System

The infrared imaging system selected for the combined system is an Inframetrics Model 600 Imaging Radiometer. This system provides a sensitivity to temperature variations of better than 0.1°C in its most sensitive mode with a specimen of uniform and relatively high emissivity. The liquid nitrogen cooled HgCdTe detector is sensitive in the long wavelength band of 8 to 12 μm. The system has a 15° x 20° field of view with an 8 to 1 electronic zoom. The system has a spatial resolution of 1.8 mrad at 50% slit contrast. It uses 200 active TV lines with 256 digital samples per line at 7 bit (128) intensity levels (8 bit with image averaging option). The system includes both hardware and software image enhancement/analysis features which include isotherm identification, contrast stretching, image averaging, image subtraction, line scan, histogram, and pseudocolor.

2. Holographic System

The holographic system selected for the combined system is a Laser Technologies, Inc. Holomatic 8000 phased-locked holographic interferometry system. The Holomatic 8000 records the reference hologram on 35mm holographic film which is processed in place. The interference pattern is then viewed in real time through a closed circuit television system which provides 600 line resolution, 2:1 interlace composite video signals. Typical exposure time for the reference image is about 10 seconds with a processing time of 10 to 15 seconds. The system uses a 35-mW HeNe laser operating in the TEM00 mode.

The selection of the phase-locked holographic system, as opposed to the more common isolation table mounted holographic approach, was made at the time of the Phase II proposal. We then recognized that the newly available phase-locked system offered the advantage of much reduced sensitivity to vibration as compared to conventional holography. This capability permits the phase-locked holography equipment to be used in many laboratory situations without a vibration isolation table. The tripod-mounted holography system provided good compatibility with the portable IR system.
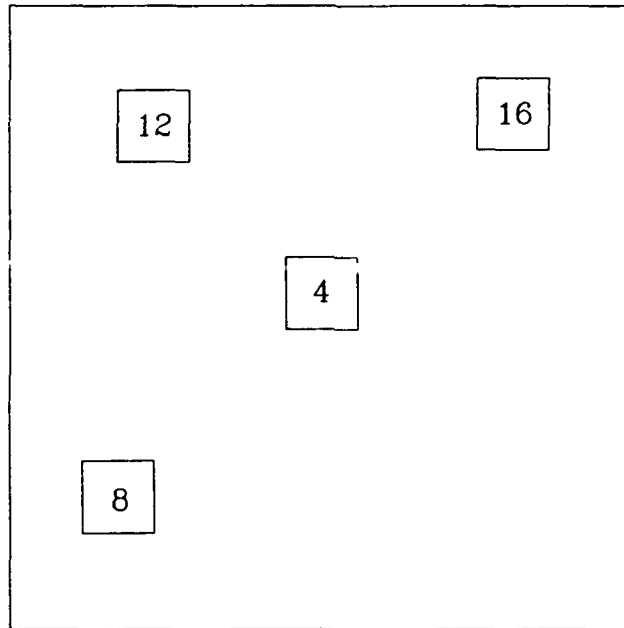
(a) Schematic of Thermographic Calibration Standard
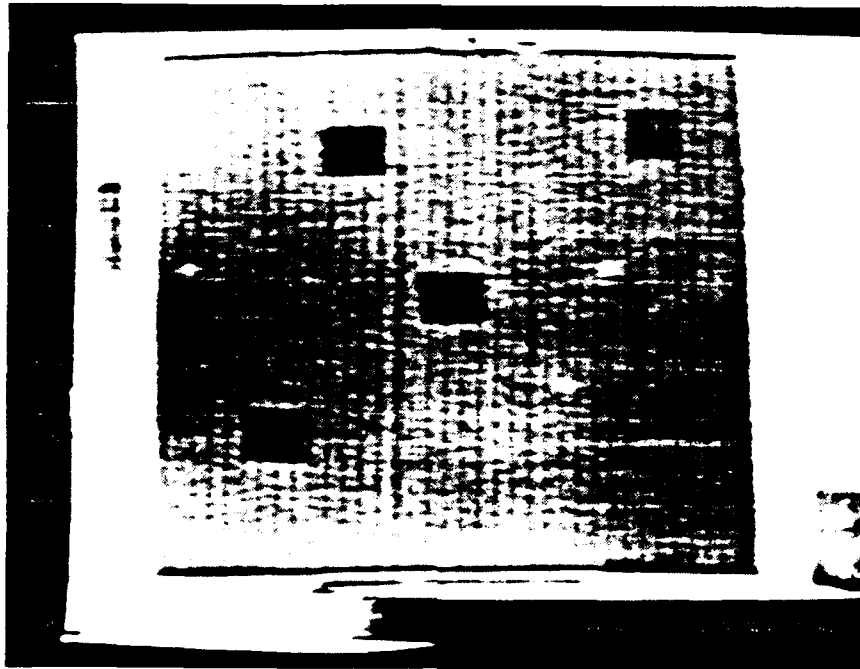
(b) Infrared Thermal Image of Thermographic Calibration Standard

Figure 10. Thermographic Calibration Standard

Thermographic Calibration Standard
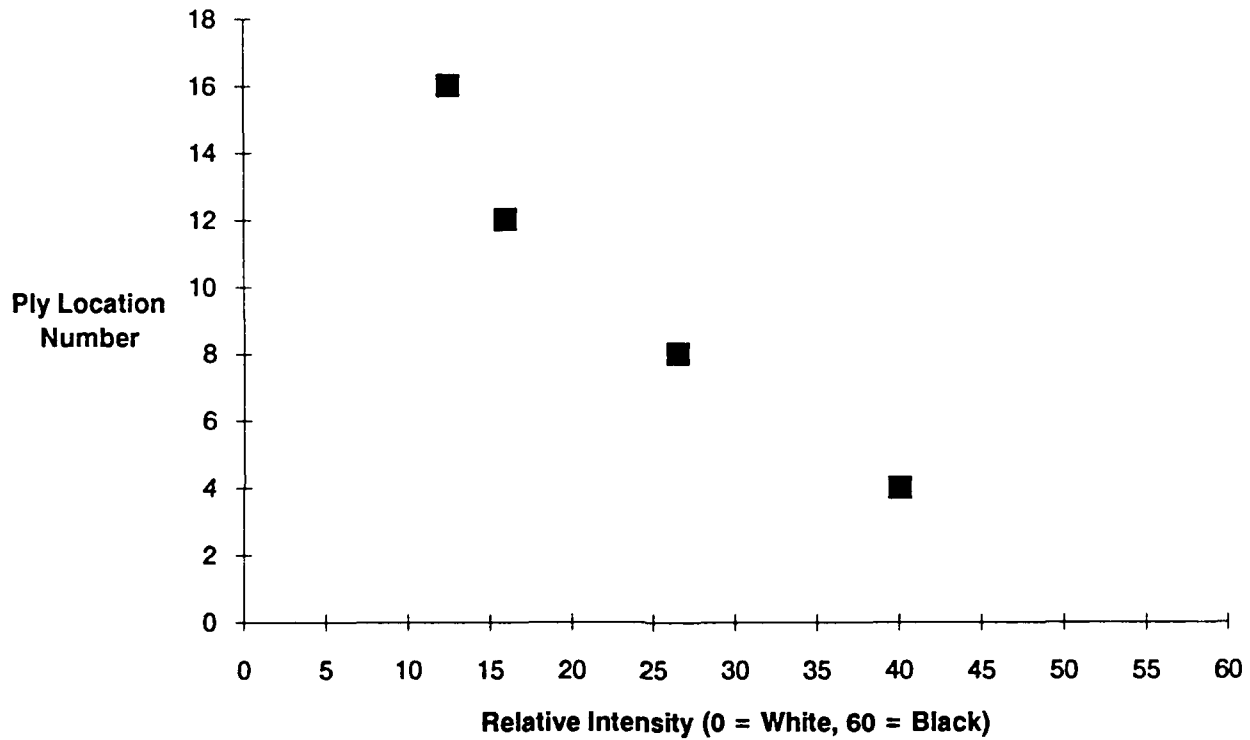
Figure 11. Decay of Surface Temperature with Flaw Depth in Calibration Standard

3. Strobe

The primary heat source selected for the combined system is a high power photographic strobe system consisting of a Speedotron model 4803 power supply and a Speedotron model 106 flash head. The model 4803 power supply can be operated at any of 13 energy settings ranging from 300 watt-seconds to 4,800 watt-seconds. The power supply offers fast and slow recycle settings. At full discharge, the recycle time is rated at 4.0 seconds for the fast recycle and 10.0 seconds for the slow recycle. The model 106 flash head is capable of handling 5,000 watt-second pulses and uses a single vented quartz flash tube. The model 106 flash head comes with an 11½-inch reflector. The flash duration at 4,800 Ws (measured at half peak amplitude) is specified at 4.0 msec. At 2400 Ws, the flash duration drops to 2.4 msec.

4. Shutter System

The high intensity of the photographic strobe heat source was found to momentarily blind the closed circuit television system in the Holomatic 8000. For this reason a shutter system was added to the front end of the Holomatic 8000 optics system. This permitted the protection of the video system from the high intensity flash and had the added side benefit of providing better protection of the unexposed holographic film from stray light, thus improving film utilization. The shutter system consists of a Uniblitz model 225 shutter with a model SD-10 shutter controller. The model 225 shutter has an aperture of 1.00 inch and has a shutter closing response time of 6.2 msec and a shutter opening response time of 6.0 msec. The model SD-10 controller can be used to operate the shutter in a normally open or normally closed mode and can be set for single fire or continuous cycling. It offers a wide range of shutter open (or closed) durations from a minimum of 9.0 msec (determined by the shutter response time) up to 99 sec, or the unit can be manually controlled for any exposure time. An additional timing interface was designed by IQI to provide an appropriate delay and sync signal to fire the strobe unit once the shutter was completely closed. (Sync signals were available for firing a strobe at full open shutter as one would normally expect with a photographic system, but not for syncing with fully closed position.)

5. Computer

We used a Compaq Portable II 80286 PC (8 MHz) for this program. The computer and software serve as the focal point for the operation scenario, with the operator performing all of the data analysis there. The Compaq is equipped with a Thermoteknix "Gram card" input/output frame grabber board. Along with the Gram card, we tested a thermal image processing software called TTX. TTX is quite useful for thermal images alone, but has distinct shortcomings when applied to interferometric images. For a software system which can process both to our satisfaction, we quickly determined that we would generate our own image processing software.

6. Software

The general processing principles employed in the Holo/IR workstation will be described in this section. A complete listing of the on-line instruction manual is included as Appendix A. The languages used in the creation of the processor are *FORTRAN*, for high-level prompting and storage functions, and *Assembly*, for the on-screen interaction and interactive data acquisition.

The processor is designed for real time or archival enhancement, storage, and display of both data acquisition modalities. In its present form, one displayed modality may be free-running while the other serves as a snapshot reference. Additionally, the free-running image

can be captured frame-by-frame and displayed frozen for the important time history information. The snapshots thus displayed for visual comparison can be representative of areas on the test sample specifically highlighted for processing. These areas will usually contain defects especially chosen for characterization using two modalities, ie. those which may not be characterized by either modality alone.

Any snapshot image may be stored on disk along with many of its characteristics. In this way, processed test data can be recalled during post-test analysis. Whereas the display of processed snapshots serves as useful qualitative information, this post-test analysis may include more quantitative processing, eg. performed using Surfer. This is explained further in the *Experimental Accomplishments* section. In any event, the raw data should be stored on video tape at the time of the test and therefore made available for processing at any time, whereupon any of the processor's features may be used just as with real-time. Our use of the processor has been largely in this video-recorded mode.

In addition to the enhancement of the raw data, the processor is also capable of enhancing differences between any of the acquired snapshots. Besides the obvious consequences for comparison of snapshots in either modality, this feature has been extremely useful for improving the visibility of low contrast interferometric fringes in the Holographic display. The result is best described as a *time derivative* feature especially effective for display of fringe (and therefore deformation height) evolution.

7. Monitors, VCR's, etc.

The workstation in its present stage of development includes several auxiliary pieces of equipment supplied by Industrial Quality, Inc. and tied temporarily to the prototype system. These include an RGB monitor and a high performance video cassette recorder (VCR). The VCR must have audio dub, or at least audio record capability. This is because the video taping of the event is accompanied by an audio soundtrack recorded either at test time or later during analysis. The soundtrack is for the purpose of identifying events during the test with the various experimental parameters such as excitation power, and experimental anomalies. The video monitor must be likewise equipped to deliver sound.

For additional capability, a second monitor and VCR and appropriate frame-by-frame synchronization between the two VCRs should be added. The synchronization condition points out an improvement in the system which will greatly facilitate pre-recorded analysis since the video playbacks of the two modalities will be able to progress together with frame (1/30 sec) accuracy and the operator can always be certain that the Holographic and IR displays represent the same moments in the course of the test. Accomplishing the synchronism involves adding a *time-code-generator* to the two video inputs.

Integration of the System/Operating Scenario

According to the Holo/IR concept, flaws in materials are detected by thermal excitation at the surface and subsequent recording of surface deformations and temperatures by holographic interferometric and thermal imaging systems respectively. The objective of testing with two modalities is twofold:

i. The combined system offers defect depth determination capability when both modalities deliver defect indications.

ii. The combined system has increased reliability of detecting defects in case only one of the two modalities offers indications.

The first condition refers back to the system of equations presented in the theory section. It is argued there that solution of the equations will yield both a defect's position and its characterization and that they become more solvable with the additional data provided by two measurement modalities.

The second condition has obvious origins. Another way of stating this condition is that the second modality provides a defect detection backup system.

We will describe the operating scenario below by way of a description of the use of the four major components of the Holo/IR workstation; the excitation source, the holographic subsystem, the infrared subsystem, and the data analysis subsystem.

1. Excitation, Holographic, and Infrared Subsystems

Setting up the three "hardware" subsystems at the testing site and a chronological description of their use is the subject of this section.

Figure 12 depicts the suggested arrangement of the inspection hardware. Of particular note is that it is helpful to position the IR camera and Holographic film windows as closely as possible. This is so that the views displayed by the two are most similar. In fact, part of the setup procedure is the registration of the two images so that the data displayed in an area on one monitor will match that displayed on the other. It is useful to have one monitor for each modality available during the test. One monitor only should be used for the registration task. The strobe head is positioned as close to the tested surface as possible without blocking either of the camera views. Another consideration in the strobe head positioning is illumination homogeneity which requires that the angle between the strobe and the test surface be as small as possible. Obviously, these two illumination conditions must be traded off.

The setup procedure for the Holomatic 8000 involves filling the developer and water supply reservoirs, connecting the fluid hoses and loading the film. These procedures are outlined in the operator's manual. The long length of (35mm) holographic film allows for the exposure of many holograms (~ 36) in succession. Some will almost certainly be needed to set the exposure time and object to reference beam ratios for optimum hologram contrast. These initial trials will consume about 15 minutes. During the data gathering phase, operation is simple, comprising the use of a single button in the Holomatic 8000 controller.

The IR camera setup procedure concerns mainly the cooling of the detector array. Several minutes before the test is to be performed, liquid nitrogen must be poured into the dewar on the camera head. The coolant serves to reduce the detector noise which is due to random motion of electrons and holes in the semiconductor detecting material. This procedure must be repeated every 1 to 2 hours since the coolant evaporates from the dewar. Besides the coolant considerations, some adjustments are provided for adjusting the sensitivity and detector bias level (to adjust temperature range and offset), but these settings default to reasonable numbers and for the most part, operation of the camera is automatic.

To use the computer analysis approach, we need to register the two inspection views. A simple technique was developed to accomplish this registration. A box is formed to outline an image detail in the holographic display. That heated detail is then centered in the box by shifting the IR camera. This alignment permits the image processing software to be used to compare the two views pixel by pixel.
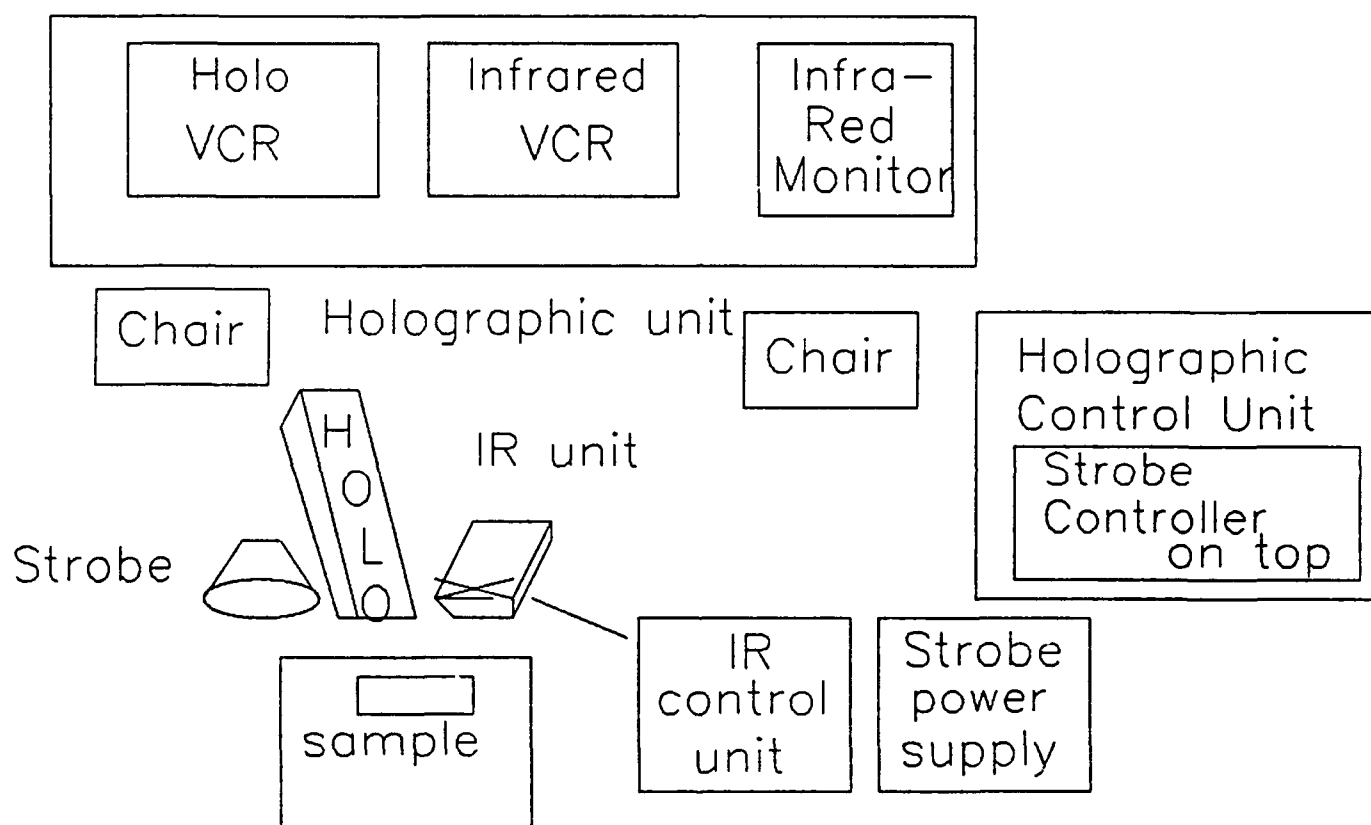
Figure 12. Equipment Schematic for Combined Holography-Infrared System

26

Once the equipment is physically set up and confirmed to be operating, actual testing can begin with the exposure of a hologram. It is necessary that the test object be in its unexcited state. The hologram is made according to the instructions in the operating manual of the Holomatic 8000. Usually the exposure time is 1-10 sec. After the film is exposed and developed, the Holomatic 8000 automatically reconstructs the hologram. The reconstruction exactly overlays the test object. If there was no perturbation in the object between exposure and reconstruction, the video output will show only the object itself. A simple test to see if the hologram was effectively recorded is to gently push one end of the laser housing. This should have the effect of introducing straight uniform interference fringes on the video screen. The laser should return to its original position.

Once it is determined that the hologram was successfully recorded, it is time to perform the test. Depressing the strobe/shutter activation button will close the shutter, flash the strobe to excite the object, and open the shutter. The most prominent effect on the holographic monitor will be the appearance of near-linear interference fringes. The warping should be an evolving effect; progressing from zero warpage at the flash through a maximum, in which the fringes are at maximum spatial frequency, and back to the preflash state. Defected areas will show as perturbations in the regular fringe pattern. The perturbations may appear at any time throughout the warp evolution. On the IR monitor, defective areas will show brighter or darker than the background, the intensity differences indicating local temperature gradients.

2. Data Analysis Examples

Several interactive processing options are available for use either in real time during the test or, using the video tapes, after the entire test sequence is complete. The results described here are predominantly of the latter type. For either case, the analysis function requires the use of the Gram card-equipped computer and an RGB-capable color monitor. The operator enters a command to begin the analysis program and is presented the option of scrolling through a tutorial-type manual which describes all of the image enhancement, storage, etc. functions available. For example, a typical methodology for analysis of the holographic data is to:

    i.   Freeze frame at a particularly interesting time during the event's evolution,

    ii.   Perform a full frame enhance function.

These procedures are each activated by depressing a function key. Other image processing functions include:

    i.   A continuous enhancement function where one area on the screen is repeatedly processed.

    ii.   A delay and save function where over a selected area several time instances during the event's evolution are saved and subsequently displayed as a group.

    iii.   Provision for interactively finding exact temperature and deformation information and for the display of the information in an isometric or contour plot (Surfer software)

Simple function key entries and prompted responses comprise the interaction commands.

EXPERIMENTAL ACCOMPLISHMENTS

Test Panel Designs/Inspection Samples

1. F/A-18 Composite Honeycomb Sample

The F/A-18 honeycomb panels were selected as the primary demonstration hardware for the combined holography-infrared inspection system. There are two panels that have been used. They are nominally identical, except that one has thick (3 inches) honeycomb core and the other thin (1/2 inch) core. The panels are shown schematically in Figure 13.

The skins are 5-ply graphite epoxy (AS4/3501-6), nominally 0.026 inch thick. The skins are adhesively bonded to the aluminum honeycomb core using FM-300 adhesive, a brominated sheet adhesive from American Cyanimid. The panels each have two weights of honeycomb core bonded together with FM-404 foaming adhesive. The core is specified by the density of the honeycomb material (2.3 and 3.1 pounds per cubic foot). Both use 0.002-inch aluminum foil. The 2.3 pcf material has 0.25-inch cells and the 3.1 pcf material has 0.187-inch cells.

Skin delaminations are made by placing CHR-3TB (0.003-inch-thick nonporous Teflon coated glass fabric) 3 plies from the outer surface. Skin to core disbonds use 6-mil Teflon coated glass fabric between the adhesive and the core. Extra adhesive is a patch of FM-404 foaming adhesive between the FM-300 and the core, and the crushed core is produced to the specified diameter before the skins are bonded on.

2. Graphite Epoxy Flat Bottomed Hole Sample

A graphite epoxy flat-bottomed hole (FBH) sample was used to evaluate the effects of flaw depth on indication presentation. The sample, shown schematically in Figure 14, consists of a 4.0 x 7.5 x 0.405 inch thick laminate. The sample contains thirteen 0.50-inch-diameter FBH's at depths ranging from 0.013 inch to 0.39 inch, and three 0.75-inch-diameter FBH's at depths of 0.018, 0.028, and 0.037 inch.

3. Graphite Silica Tube

A graphite fiber silica glass matrix tube was supplied by the COTR for evaluation on the combined system. The sample is a 12-inch-long cylinder, 2.5 inches in diameter with a 0.25-inch wall thickness. The tube contained a number of porous areas in the matrix.

4. Other Test Samples

A variety of other inspection samples were examined. The ones reported here include those that provided some unusual or significant results. Inspection samples used for illustrations or discussion in this report include an impact-damaged composite tube (see Figure 2), a Kevlar face sheet composite laminate (16 plies) containing Grafoil inserts at ply depths 4, 8, 12 and 16 to simulate defects (this sample was used for the calibration of the pixel-value IR depth measurements, Figure 10) and a brazed, felt-metal abradable engine seal sample used to illustrate the excellent holographic sensitivity to defects in this good conductivity material (an inspection result is shown in the Discussion and Conclusions section).

Additional samples were examined, including a composite inlet vane provided by the Air Force.

CALIBRATION POINT
P2 UPPER AND
LOWER SURFACES

CALIBRATION POINT
P2 UPPER AND
LOWER SURFACES

CALIBRATION POINTS

CRUSHED CORE

EXTRA FM404 ADHESIVE

CHR-6TB TEFLON
COATED FABRIC

CHR-3TB
TEFLON
COATED
FABRIC

12.00
2.00
2.00
4.00
2.00
1.50
1.50
2.00
2.00
2.00

1.0 DIA

1.5 DIA   1.00 X .00

0.50 X 0.50

1.0 DIA

1.5 DIA

0.50 X 0.50

0.375 X 0.375

0.25 X 0.25

1.50

1.50

A

B

12.00

3.1 POUNDS PER CUBIC
FOOT HONEYCOMB CORE

FM404
CORE SPLICE

2.3 POUNDS PER CUBIC
FOOT HONEYCOMB CORE

LEGEND

HONEYCOMB CORE REFERENCE
STANDARD THICKNESS (T)

PART NUMBER	T=
74D111295-1001	3 INCHES
74D111295-1005	1/2 INCH

T

FIVE PLIES OF 5 MIL
PREPREGNATED GRAPHITE
EPOXY FABRIC, UPPER
AND LOWER SURFACES

LOCATION OF
CRUSHED CORE,
FM404, AND CHR-6TB

1 LAYER FM300

HONEYCOMB CORE
T = HEIGHT 1/2,
AND 3 INCH

A

CHR-3TB LOCATED
IN UPPER SKIN THREE
PLIES BELOW MOLD LINE

B

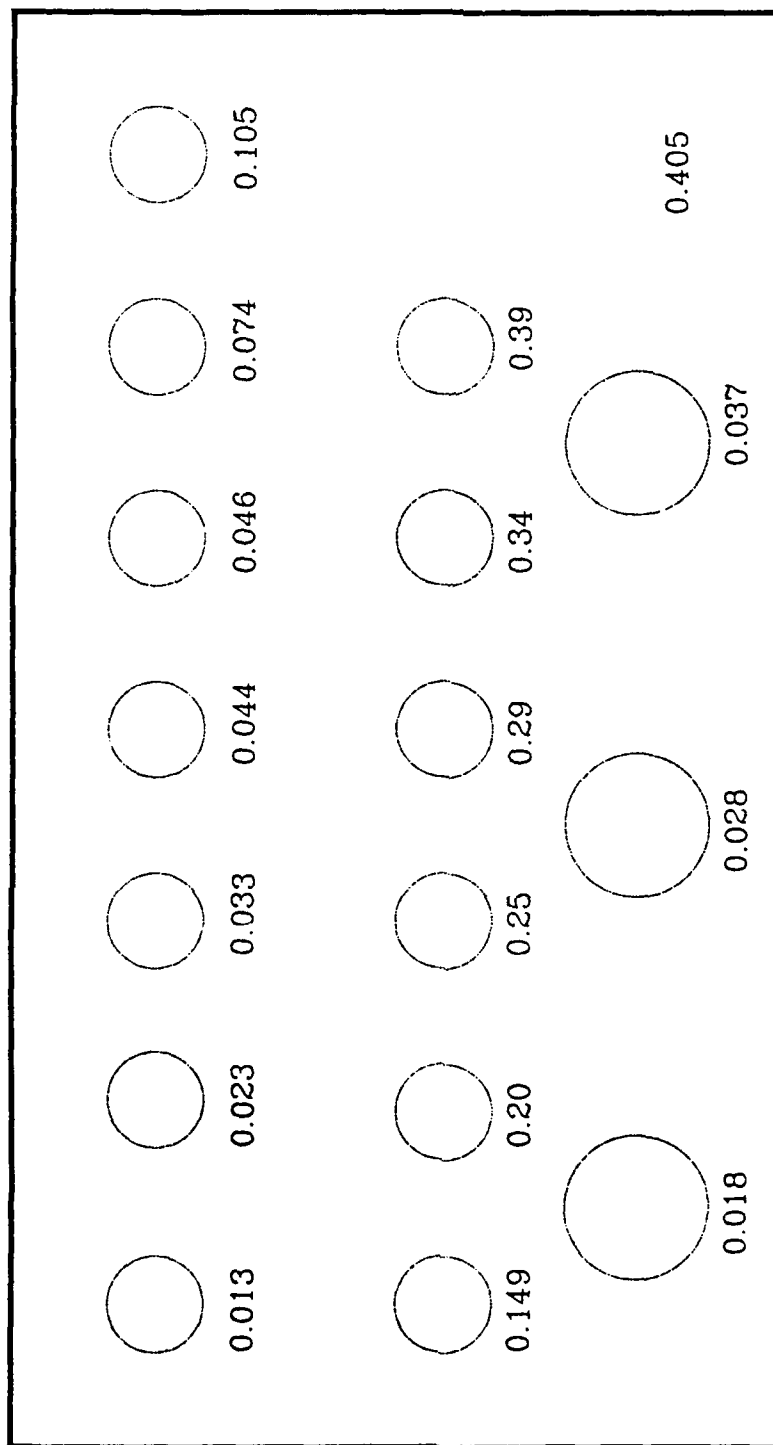**Figure 13. F/A-18 Graphite Epoxy Skinned Aluminum Honeycomb Sample**

29

Figure 14. Graphite Epoxy Flat-Bottomed Hole Sample

Equipment Test Plan

The Equipment Test Plan is provided as Appendix B. The plan describes the performance specifications of the holographic and infrared imaging subsystems, describes the combination of the two subsystems in a test configuration and defines the test criteria for that F/A-18 honeycomb sandwich panel. The test plan anticipates that the holographic subsystem will be able to detect all flaws 1/2 inch or larger in this panel and the infrared system will provide detection of all defects including the 1/4 inch delaminations.

Experimental Developments

Our early efforts concentrated on the use of the Holo and IR systems side-by-side to obtain defect indications on samples with known flaws using both modalities. Hot air heating was used primarily as the excitation method. We did generate some data confirming the feasibility of the side-by-side approach. However, it became clear after the data analysis that in important ways neither the excitation nor the analysis was quantified.

In another series of experiments, some control was provided by the use of a 4-kW quartz lamp which we configured to illuminate the sample with its linear beam by computer controlled scanning of a deflection mirror. During the approximately 10-second scans, each sample area was roughly calculated to have received some 0.5 sec X 4 kW = 2 kJ of heat energy input. The excitation energy was sufficient to reveal defects on both modalities. Examples shown in Figures 15 and 16 illustrate holographic and infrared detection of several defects in the F/A-18 honeycomb panel.

On analysis, it became clear that, although defect indications were present on both Holo and IR displays, it was difficult to make quantifiable connections between the two. This is because the behavior which provided this connection occurs within a few hundred milliseconds of the excitation. This brought recognition for the need of a high powered (5 kJ in 4 millisec) strobe flash unit. With the flash unit, a controlled amount of heat is delivered to the sample in approximately 4 ms without scanning.

Further experiments with the strobe, shutter, and supporting electronics were aimed at a full characterization of the excitation technique in terms of its interaction with the imaging subsystems, especially the holographic imager. The strobe flash unit worked well for this purpose. However, the bright light source saturated the response of the holographic detector and left it ineffective for several seconds following the flash. A shutter was needed to block the light flash and then open the aperture to permit the holographic response. Some electronic circuitry design was necessary to synchronize the strobe and shutter subassembly. A shutter and controller were obtained and customized to suit the Holo/IR system by carefully timing the shutter's closing to coincide with the strobe's excitation signal, and its opening to occur at a preset time when the light intensity returned to a preflash level. A time delay of 180 msec proved useful. This allowed ample time for the shutter to close before the flash fired and blocked the main flash and afterglow of the strobe lamp that persisted for times on the order of 100 msec. The 180-msec time period was used for all subsequent experiments.

Figure 15. Holographic Interference Image of F/A-18 Honeycomb Panel
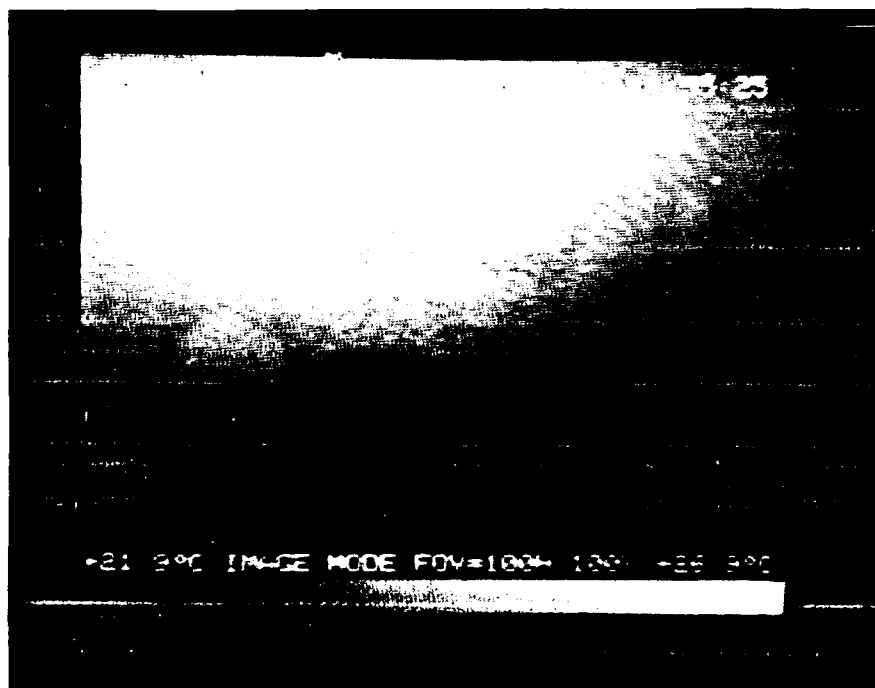
Figure 16. Infrared Image of Same Area of F/A-18 Honeycomb Panel

The shutter closed time must be kept to a minimum to ensure detection of rapidly fading indications. An example of such indications comes from the series of tests on the graphite silica tube. With this sample, good results were obtained at the full energy setting of 4,000 watt-seconds. Several examples of infrared results for the graphite-silica tube are shown in Figures 17 and 18. Figure 19 shows the layout of the images on the specimen surface. The images in Figure 17 are taken at 90 degree increments around the circumference of the tube on the end with white hash marks. These marks served to provide a 0 degree reference. Figure 18 repeats this procedure for the opposite end of the tube. Each of these images was produced with a single 4,800 watt-second pulse from the strobe. This pulse rapidly warmed the surface which then rapidly cooled. Within 2.5 to 3.5 seconds from the heat pulse, the indications had generally faded completely. The indications first became visible as soon as the afterglow of the flash tube ended. The afterglow persisted for about 0.3 second. Depending on the setting of the infrared scanner, the flaws generally first become visible somewhere between 0.3 and 1.0 seconds. Since the material in the tube is rather stiff and thick walled, and the porosity/void flaw type is not particularly well suited to holographic inspection, no indications were seen with this modality.
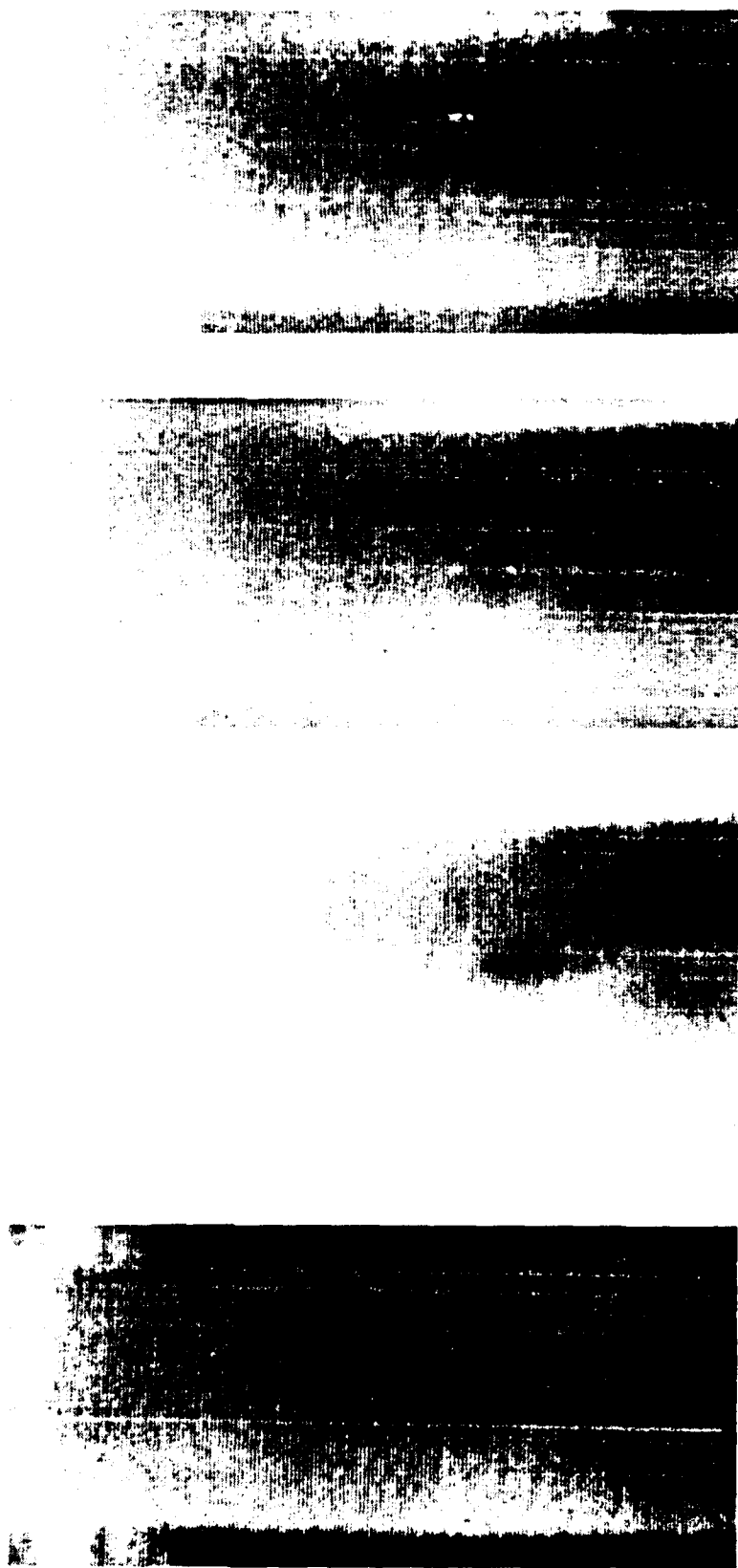
In some of the early tests with the high intensity strobe, it became clear that the samples were overexcited. Overexcitation causes problems in both displays; in the Holographic, warping causes fringes of excessive spatial frequency, in the IR, the display quickly saturates over defect areas because of the extremely fast surface temperature increase, and timing information immediately after the heat flash is lost. On the other hand, overexcitation produces very high surface temperature contrast and large deformations resulting in striking displays. In this case, however, the two displays are performing essentially independently. Examples are shown in Figures 20 and 21.

The effectiveness of the strobe-shutter improvement in the data gathering procedure was particularly significant as a consequence of our ongoing image enhancement efforts, which had just become operable at about the same time. With the enhancements, for example, small surface temperature differences which are nearly indiscernible in the raw data become clearly visible after processing. For the holographic display, the processing significantly improves the fringe contrast. One consequence of the improvements in both data collection and image processing, was the ability to show defect indications as they evolved within 200 ms of the flash excitation.

We were able to use the data on the graphite epoxy flat bottom hole sample to demonstrate defect depth detection capability using the data from each modality alone. In these demonstrations, holes at particular depths are outlined and a time history of surface deformation and temperature since the excitation is compiled by the IQI Holo/IR image processing software.

The results clearly show from each modality alone that "delaminations" at greater depths reveal themselves later than those near to the sample surface, and therefore that relative depth information can be obtained. Figure 9 is an example of this for the IR modality. Some qualitative demonstrations of the "time space cross-correlation" capacity of the Holo/IR system were also possible on analysis.

The analysis highlights the crushed-core defect on the F/A-18 panel. Both Holographic and Infrared time sequences on the crushed core defect area have been generated. The Holographic sequence clearly shows a deformation over the defect at time, t = 0 and a flattening of the deformation as time goes on. A typical result is included as Figure 22. In the figure, the six boxes are contrast-enhanced versions of the area over the 0.028-in-deep hole of the FBH sample. Each of the six "snapshots" were taken at a

Figure 17. Infrared Images of Graphite/Silica Tube (End with Hash Marks)

0° View   90° View   180° View   270° View

34

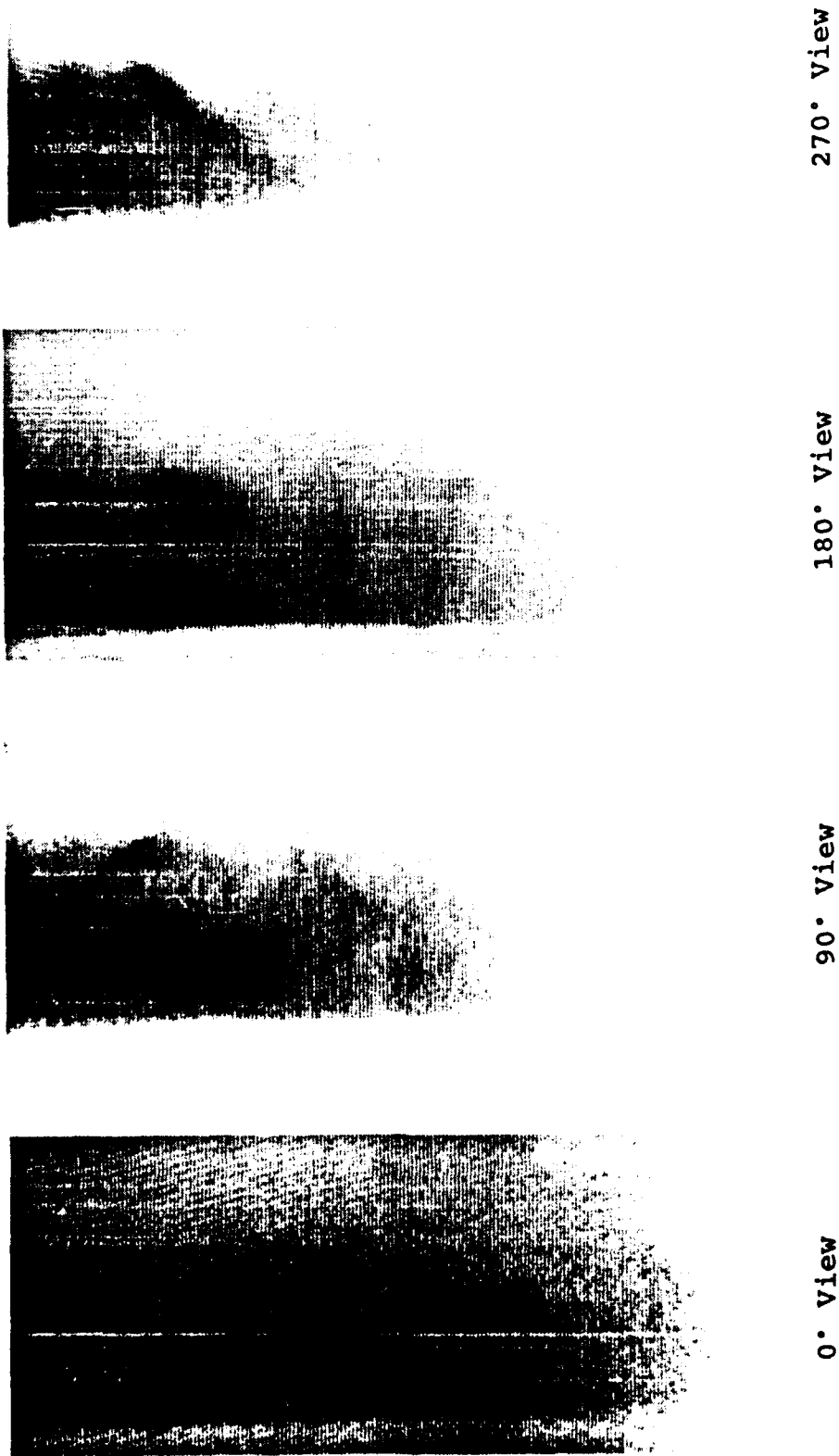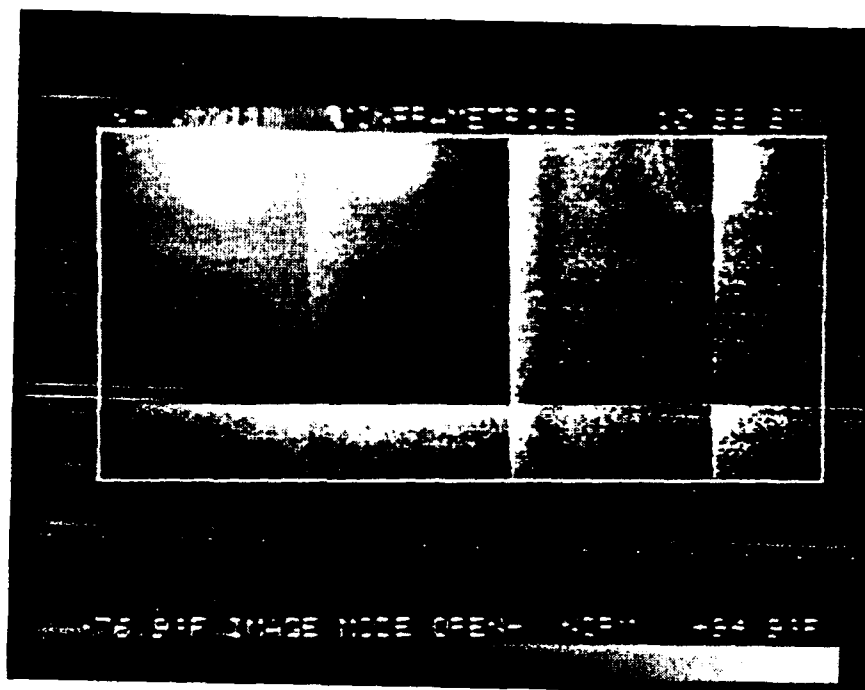0° View   90° View   180° View   270° View

Figure 18. Infrared Images of Graphite/Silica Tube (End with #3 Marking)

Figure 20. Overexcited Infrared Image of F/A-18 Panel

Figure 21. Overexcited Holographic Image of F/A-18 Panel

different time. In this case, the times relative to the flash excitation are 0.19, 1.11, 2.03, 2.95, 3.87, and 4.79 sec, for the boxes running from top left, to bottom left, to top right, to bottom right. Note then that for this example, even for a slightly deeper and larger delamination, the holographic indication appears much sooner than that for the IR, and that the deformation recedes much quicker than the time required for surface temperature equalization.

Quantitative analysis of the height/temperature versus time history is possible with the Surfer package. This is recommended for more in-depth analyses.

With the successful demonstration of the Holo/IR workstation, we were in a position to perform preliminary demonstrations of the LTI Electronic Shearography imaging system. As mentioned, the combination of Shearography and Infrared images could prove to be a successful method of defect characterization as well. Moreover, the simple setup and operation of the LTI ES 9100 Shearography unit may make it superior to the Holomatic 8000 as a companion to the infrared equipment in the IQI Holo/IR workstation. The shearography is less sensitive to vibration. Therefore the Shearo/IR combination could be considered for field inspections. Some Shearography results are therefore included on the video demonstration tape. We must remember that it was not within the scope of this project to fully determine the feasibility of the Shearo/IR combination; therefore, the Shearography results are not accompanied by corresponding IR results in the presentation.

Shearography defect indications reveal the defect in a slightly different way than Holographic Interferometric indications. In particular, whereas the holographic display shows fringes dependent upon the surface height, shearography indicates surface *slope*. The display is somewhat difficult to interpret for this reason. Furthermore, since in general the slope changes faster than height, then for the same yardstick of measurement (wavelength of light), the shearography result will be less sensitive (small slopes don't show up regardless of the height). However, shearography does offer the advantage of reduced warpage effect, since a sloped warped surface shows a constant shearographic intensity. Indeed, our image processing software as designed for the Holo/IR combination features a *temporal slope* (time derivative) to similarly accomplish cancellation of the illumination nonuniformity which causes warpage. A snapshot example of the shearography display is included as Figure 23.

Image Processor Development

1. Interactive Graphics Design

The software project took on the form of an image processor when it was determined that some preprocessing of the holographic data were necessary for adequate operator interaction with the screen. Once enhancement activities began, we gained full control of the flow of data from the acquisition to the display monitor, whereupon we provided the feature of simultaneous display of live and frozen imagery.

Further improvements concentrated on providing accurate timing information and using it for enhanced visual effect. It was determined that this effect was superior in a practical sense to the Surfer concept. Furthermore, Surfer did not provide sufficient post-processing capability to make it fully compatible with our specifications for the Holo/IR output imagery. Therefore, the Surfer isometric perspective display was abandoned for the IQI interactive image enhancement package.
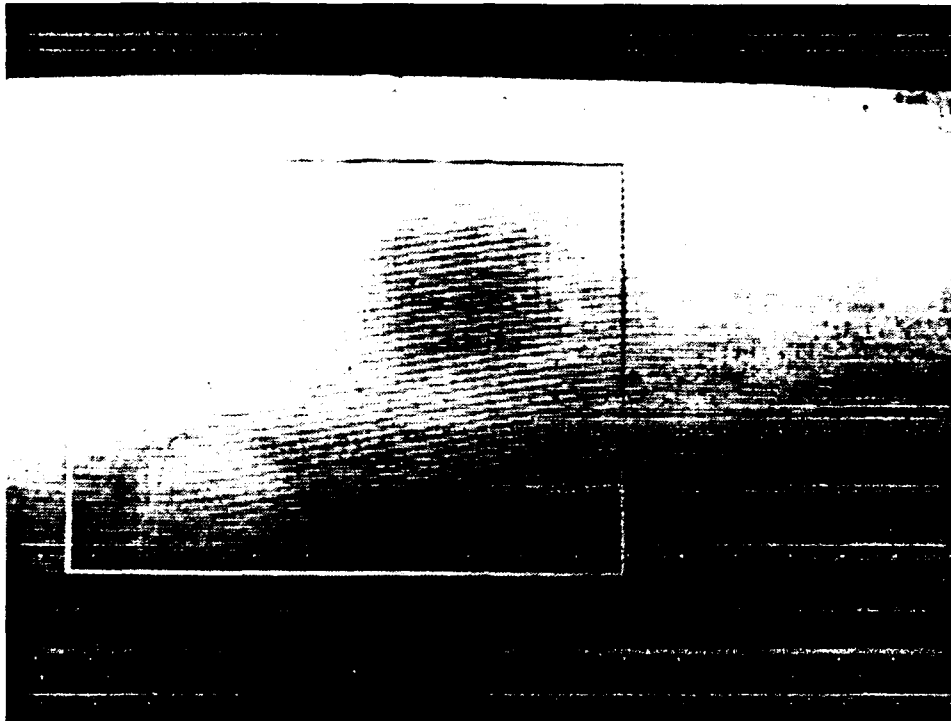
Figure 24. Thermal Image of Crushed Core and Extra Adhesive Defects
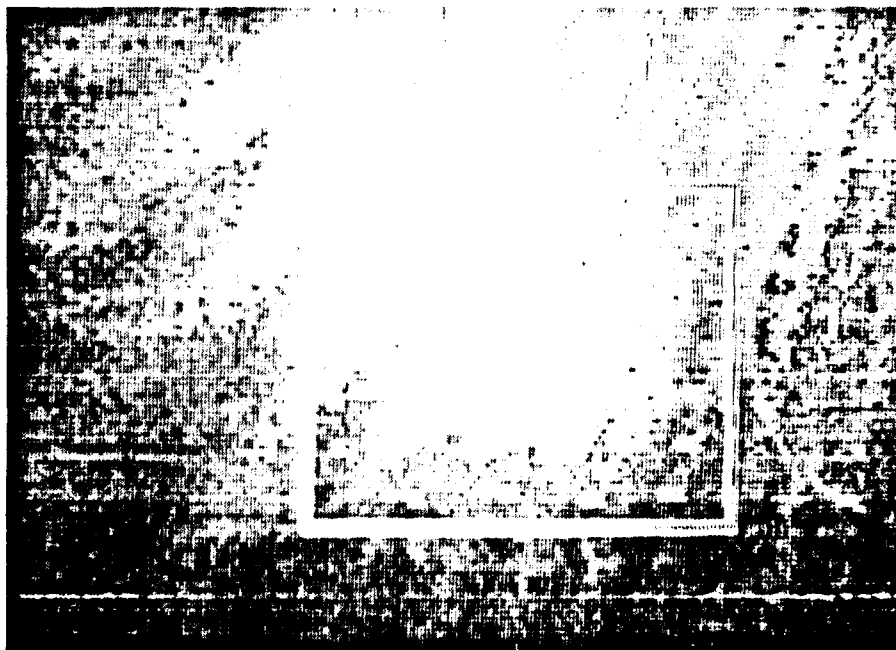
Figure 25. Video Hologram with Graphic Overlay
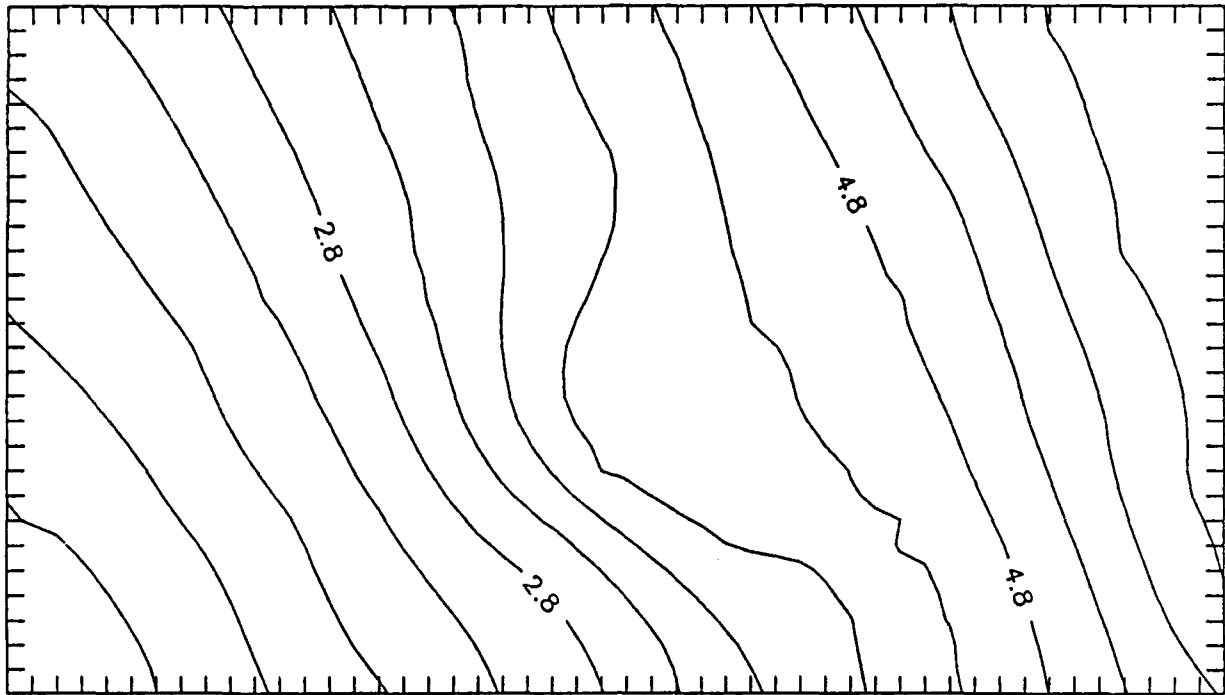
Figure 26. Surface Topographic Map Produced by Surfer
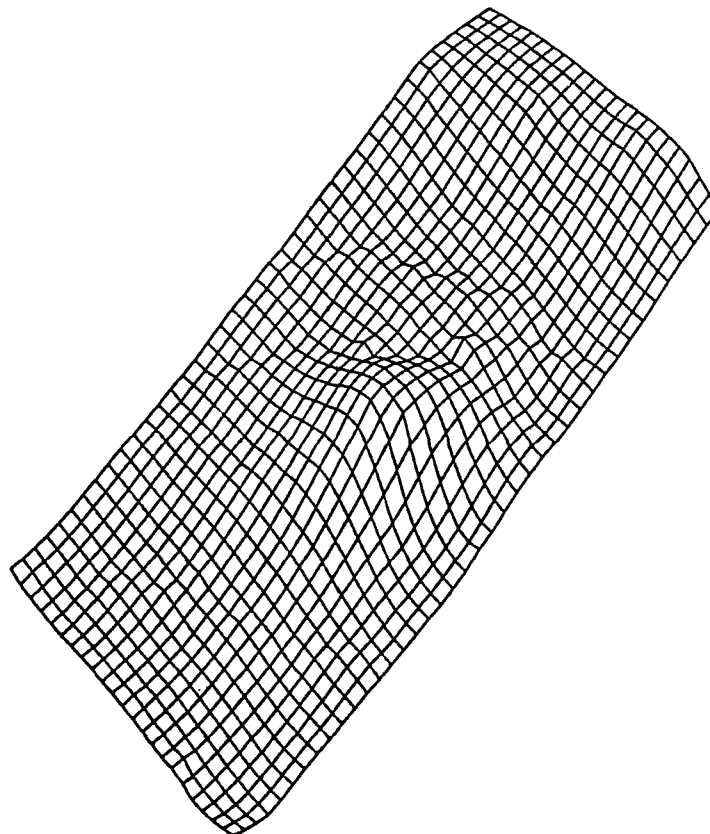
Figure 27. Surface Displacement Map Produced by Surfer

43
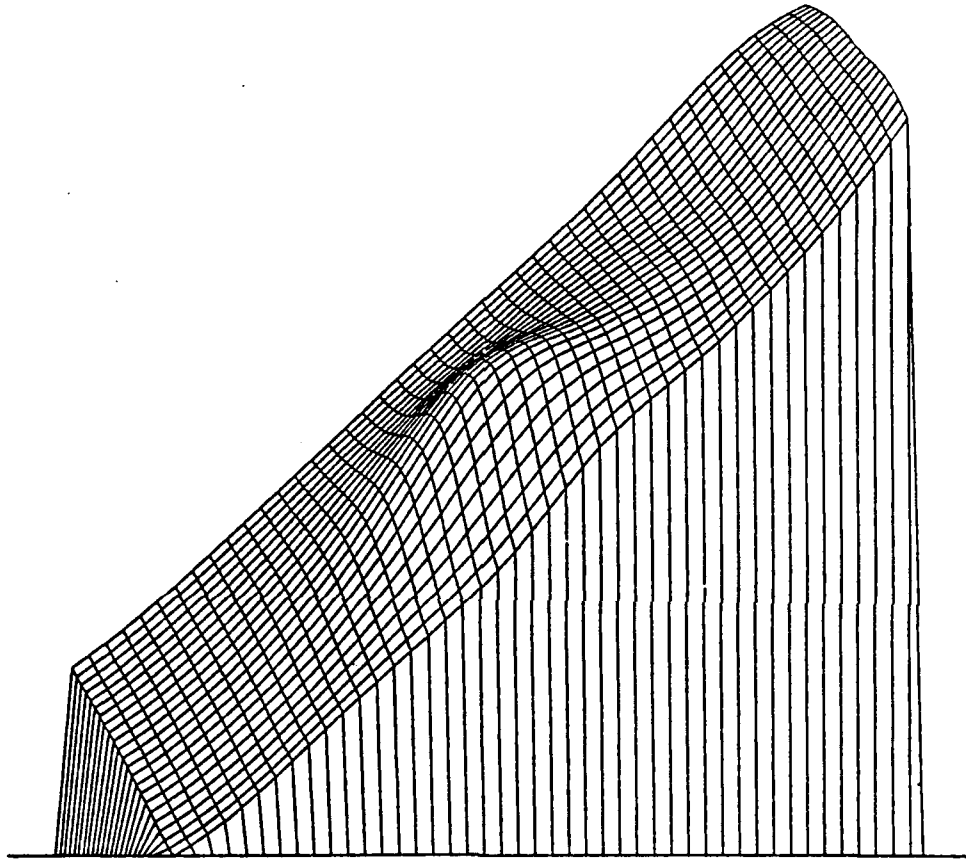
Figure 28. Enhanced Surface Displacement Map

Figure 24 showed a thermal image of a portion of the F/A-18 honeycomb panel in an area containing crushed core and excess adhesive. The crushed core shows as hotter (lighter) and the added adhesive shows as cooler (darker). The area of interest is outlined with a rectangle. Only data within that area of interest will be considered for inclusion in the data file. Toward the top of the area of interest are indications of crushed core on the left and added adhesive on the right. At the bottom edge of the box are much lower contrast indications of each flaw type. These data were read with a skip factor of 1. Thus every other data point (2^1) on every other row was saved. This file was input into the Surfer program for three-dimensional plotting. The results are shown in Figure 29. A peculiarity of the data handling technique causes the data to be mirrored left to right. Thus the crushed core indications now appear on the right and the added adhesive on the left. This is because "X-axis" values are read as pixel numbers increasing from left to right, while "Y-axis" values are read as line numbers increasing from top to bottom, thus producing an unconventional coordinate system.

PROSPECTS FOR COMMERCIALIZATION

This investigation has shown that the combined inspection system offers advantages in terms of improved detection and characterization of defects and in terms of quantitative defect depth information. Therefore, we see a market for the combined inspection system.

Plans are to address that market in combination with Laser Technology, Inc. The infrared capability makes a logical addition to the existing LTI line of holography and shearography equipment. LTI has manufacturing and marketing capability for this type of inspection equipment. Also, as subcontractors during this development program, LTI personnel are familiar with the equipment and its applications.

Some additional product development remains to be done. This includes an improved software package for control and analysis and a more commercial packaging of the hardware. At the same time as we are continuing these developments, LTI will begin to offer the infrared addition as an option for current optical inspection equipment customers. In addition, LTI will initiate marketing of the combined system directly. The video tape made to demonstrate the equipment and its operation for the Air Force should prove to be a helpful marketing aid.

SAFETY ISSUES

A Safety Assessment Report has been submitted. The report is included here as Appendix C.

The major safety issue is that we must take precaution to not look directly into the laser incorporated in the holography unit. The 35-mW HeNe laser is a Class IIIB laser. This requires restricted access to the unit during operation.

With reasonable precautions, as discussed in Appendix C, there should be no problem in using this holographic-infrared equipment safely.
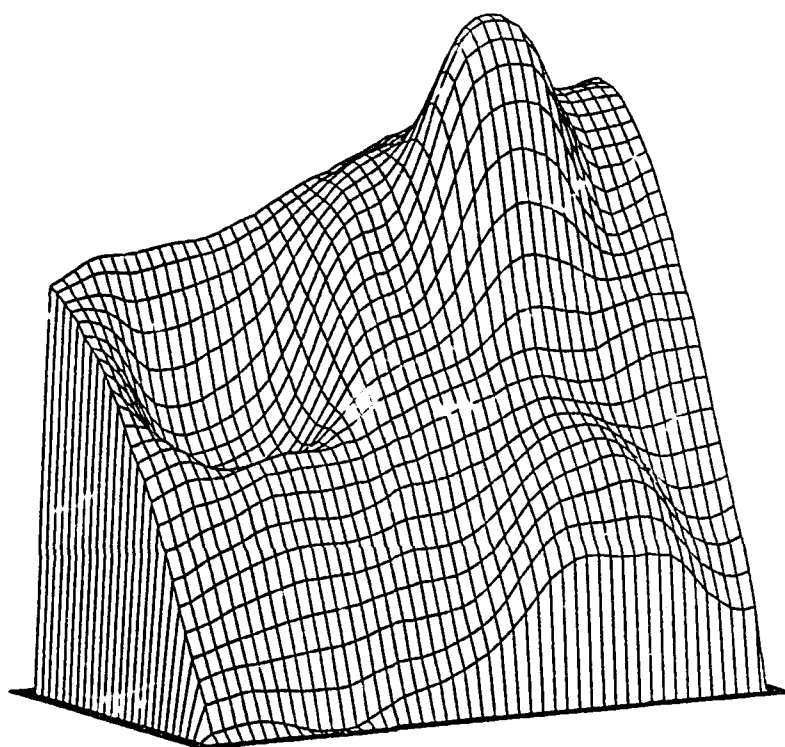
Figure 29. Three-Dimensional Rendering of Thermal Image in Figure 24

DISCUSSION AND CONCLUSIONS

The results of this program indicate that the Holography Infrared combination does deliver improved defect-detection capability. The theory shows that the two inspection modalities, combined with reasonable boundary conditions, permit a quantitative analysis for an arbitrary inspection sample. We have shown experimentally that both holographic and infrared indications are evident for a variety of cases and for a variety of samples. To the extent possible, we have accumulated quantitative data on parallel displays of single events. These data have yielded in two display modalities, and for two independent material phenomena both the defect's presence and the time to first detection. With this information, and armed with the theoretical response predictions, the defects can be characterized to a greater degree than with either display alone.

As an example of this conclusion, consider the present methods of defect depth determination using infrared results alone. These methods are described in the Infrared Thermography section of this report. According to the discussion there, one can accurately determine absolute defect depth only with very tight control of the excitation condition and with a reference case at hand. Furthermore, the defect type must be known beforehand. What we have shown in this project is that using the Holo/IR combination approach and some basic theory, it is possible to gain defect depth information for an unknown excitation intensity, no reference sample, and no prior knowledge of the material composition or defect type. Defect characterization can follow the acquisition of two sets of time-dependent sequences of events following an excitation pulse, namely the holographic interferogram and the infrared surface temperature display.

Much of the work leading up to these conclusions involved improvements in data presentation strictly for the purpose of comparing and contrasting, *correlating* the two independent modalities. The objectives were both to provide a framework wherein the correlations would yield additional information not available in either display alone and to make a clear case for the system's use as a redundant inspection technique, where defect indications not available as surface temperature variations, for example, would be available as displacements. This latter objective is valid, as indicated in the discussions of several situations where one or the other inspection modality offered improved response. Examples include detection of small defects in abradable engine seals, as shown in Figure 30, and detection of delaminations between two foam layers. These applications are better suited to holographic detection as compared to infrared imaging. On the other hand, the IR system gave good detection capability for small area composite delaminations, 12 mm and less, a size range that often presents problems for holographic testing. See Figure 31 in which skin delaminations 6, 9, and 12 mm across are clearly detectable (although these indications were quickly fleeting). None of these flaws were detected in the hologram. This problem is further accentuated for stiff skin assemblies. For these classes of defects, then, the Holo/IR combination presents a crucial redundancy in data collection, without which the defect indication may be missed.

Another conclusion reached after extended experience with the phase-locked Holo system and more recent experience with newly available electronic shearography is that the shearography-infrared combination (Shearo-IR) offers broader application possibilities. The phase-locked Holo system, selected several years ago, offers the advantage of tripod-mounted laboratory use. In this environment, the phase-locked Holo system provides inspection data and does not require a vibration-isolation table as do conventional holographic systems. Nevertheless, operation of the phase-locked Holo system requires extended control of environmental conditions. The shearography system, on the other hand, offers true tripod-mounted operation; it is much less sensitive to vibration because the optical system uses the sheared double image of the part to form reference and object fields.
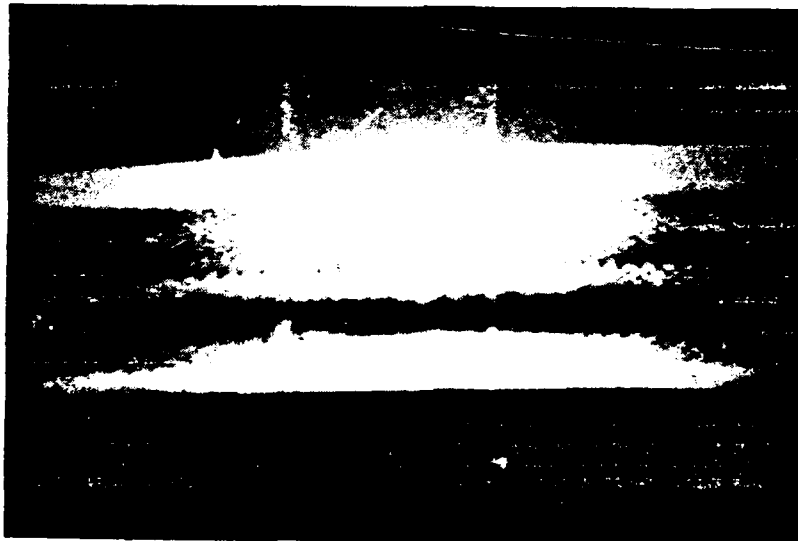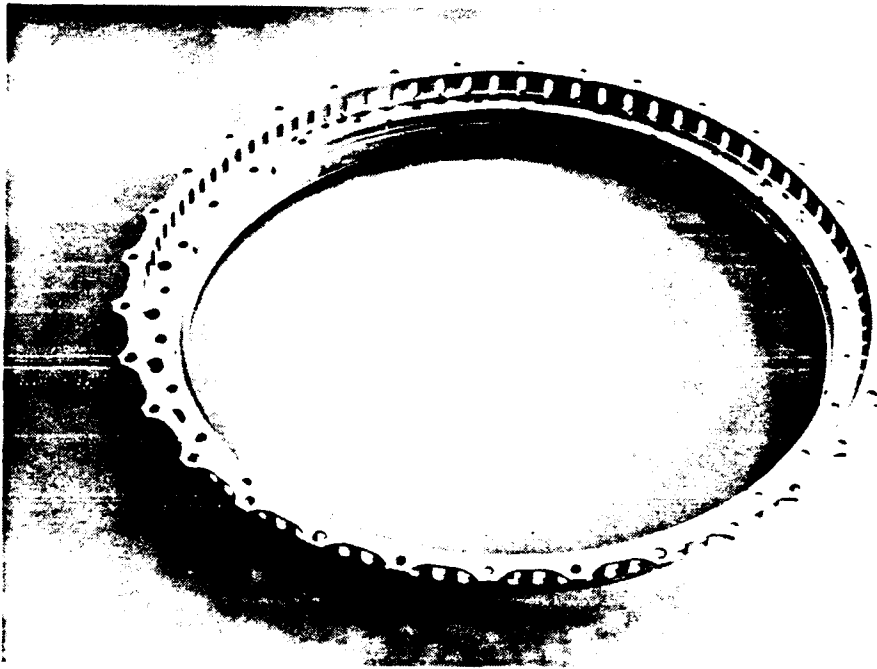
Figure 30. Hologram of Aircraft Engine Abradable Felt Metal Seal
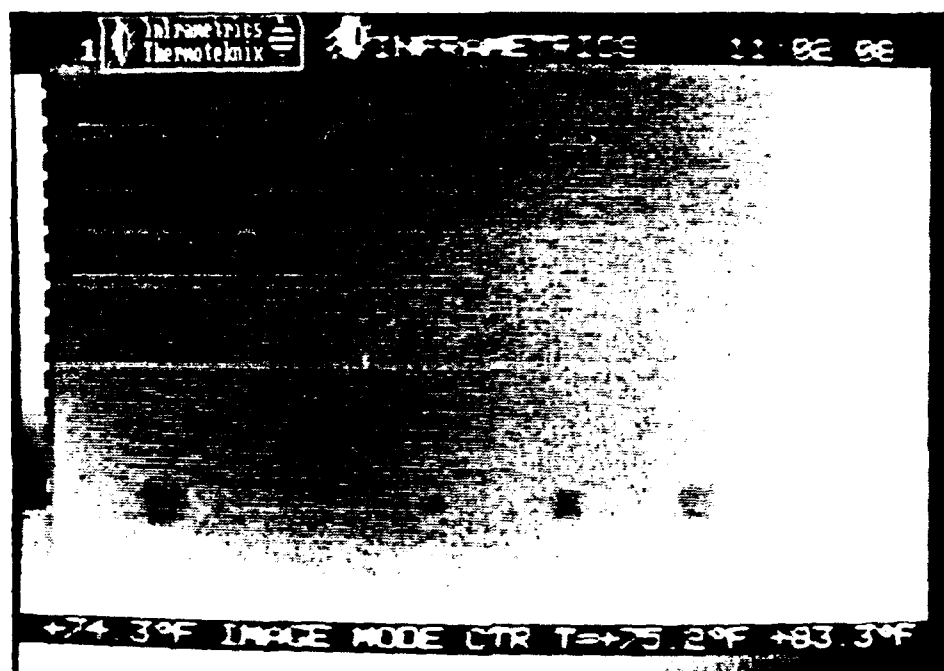
Figure 31. Infrared Image of Small Skin Delaminations in F/A-18 Honeycomb Panel

Therefore, the Shearo-IR inspection systems can be used in many practical environments; in the factory or in a field location. Our recommendations follow from these analyses, as follows:

1. Holo-IR inspection systems combine the high sensitivity of both inspection methods when used on a vibration-isolation table.

2. Holo-IR inspection systems provide good inspection capability in a well controlled laboratory environment with the IR system combined with a phase-locked Holo unit on a tripod.

3. Shearo-IR inspection systems combine the two inspection modalities well. Inspections can be accomplished under a broad range of conditions, both in the plant and in the field.

REFERENCES

1. Ennos, A.E., "Optical Holography and Coherent Light Techniques," *Research Techniques in Nondestructive Testing*, R.S. Sharpe, editor, Vol. 1, 155-180, Academic Press, London and New York, 1970.

2. Erf, R.K., *Holographic Nondestructive Testing*, Academic Press, New York, 1974.

3. Vest, C.M., *Holographic Interferometry*, Wiley, New York, 1979.

4. Ostrovsky, Y.I., M.M. Butuzov and G.V. Ostrovskaya, *Interferometry by Holography*, Springer Verlag, Berlin, 1980.

5. Jones, R. and C. Wykes, *Holographic and Speckle Interferometry*, Cambridge University Press, 1983.

6. Vest, C.M., "Holographic NDE: Status and Future," Report NBS-GCR-81-318, National Bureau of Standards, Washington, DC, 1981.

7. Burchett, O.J., "Analysis Techniques for the Inspection of Structures by Holographic Interferometry," *Materials Evaluation*, 30, No. 2, 25-31, 1972.

8. Harris, W.J., and D.C. Woods, "Thermal Stress Studies Using Optical Holographic Interferometry," *Materials Evaluation*, 32, No. 3, 50-56, 1974.

9. Edenborough, N.B. and D.J. Monnier, "Holographic Inspection of Thin Cover Sheet Bond Quality on Turbine Components," *Materials Evaluation*, 39, No. 7, 643-646, 1981.

10. Ebbeni, J., editor, "Industrial Applications of Holographic Nondestructive Testing," Proc. SPIE, Vol. 349, 199 pages, Society of Photo-Optical Instrumentation Engineers, Bellingham, WA, 1982.

11. Sarma, A., T. Kutty, P. Mani, V. Ravindran, A. Sankaranarayanan and S. Pillai, "Holographic Nondestructive Testing of Propellant Grains," *Materials Evaluation*, 42, No. 8, pp. 1025-1028 and 1034, 1984.

12. Barbier, P., "Holography -- The Nondestructive Testing of Composite Structures," Proc. Qualtest-3 Conference, Paper IQ84-651, Society of Manufacturing Engineers, Dearborn, MI, 1984.

13. Querido, R.J., "New Applications of Holographic Nondestructive Testing of Advanced Composites in Aerospace Constructions," 11th World Conf. NDT, Vol. 1, 461-468, American Society for Nondestructive Testing, Columbus, OH, 1985.

14. Paoletti, D., S. Amadesi and A. D'Altorio, "A Fringe Control Method for Real-Time HNDT," *Optics Communications*, 49, No. 2, 98-102, 1984.

15. Wolfe, W.L. and G.J. Zissis, "The Infrared Handbook," Office of Naval Research, Dept. of the Navy, Washington, DC, 1978.

16. Henneke, E.G., II and T.S. Jones, "Detection of Damage in Composite Materials by Vibrothermography," *Nondestructive Evaluation and Flaw Criticality of Composite Materials*, ASTM STP 696, R.B. Pipes, editor, American Society for Testing and Materials, 1979.

17. Infrared issue, E. Wormser, editor, *Applied Optics*, 7, No. 9, 1968.

18. Wilson, D.W. and J.A. Charles, "Thermographic Detection of Adhesive Bond and Interlaminar Flaws in Composites," *Experimental Mechanics*, 21, pp. 276-280, 1981.

19. Hsieh, C.K., X.A. Wang and S.L. Yang, "Infrared Scanning Thermography for a Quantitative Detection of Cavities," *Journal of Nondestructive Evaluation*, 3, No. 2, pp. 99-109, 1982.

20. Mertz, E., "The Application of Infrared Thermography for Maintenance in the Iron and Steel Industry," *Revue Generale de Thermique*, 21, No. 251, pp. 909-911, 1982.

21. Vavilov, V.P. and R. Taylor, "Theoretical and Practical Aspects of the Thermal Nondestructive Testing of Bonded Structures," in *Research Techniques in Nondestructive Testing*, R.S. Sharpe, editor, Vol. 5, pp. 239-279, Academic Press, London and New York, 1982.

22. Cohen, J., "Elements of Thermography for Nondestructive Testing," NBS Technical Note 1177, National Bureau of Standards, Washington, D.C., 1983.

23. Papadakis, E.P., H.L. Chesney and R.G. Hurley, "Quality Assurance of Aluminum Radiators by Infrared Thermography," *Materials Evaluation*, 42, No. 3, pp. 333-336, 1984.

24. Wilson, D.W. and S.I. Guceri, "Thermographic Nondestructive Evaluation of Steel-Polypropylene Laminates," *Journal of Nondestructive Evaluation*, 4, No. 1, pp. 13-21, 1984.

25. Reynolds, W.N. and G.M. Wells, "Video-Compatible Thermography," *British Journal of Nondestructive Testing*, 26, No. 1, pp. 40-44, 1984.

26. Hinton, Y.L., R.J. Shuford and C.G. Pergantis, "Applications of Real-Time Thermography for NDT of Composites," Conference Thermosence VII, Cambridge, MA, November, 1984, Society of Photo-optical Instrumentation Engineers, Bellingham, WA.

27. Rogovsky, A.J., "Quantification of Pulsed Infrared Thermography for Composites," *11th World Conference on Nondestructive Testing*, Vol. 1, pp. 376-383, 1985.

28. Gallagher, D.J., "NDI of Graphite/Epoxy Composite Materials Using Computer-Aided Thermography," *11th World Conference on Nondestructive Testing*, Vol. 1, pp. 420-426, 1985.

29. Berger, H. and D. Froom, "A Comparison of NDT Methods for Honeycomb Bond Inspection," *11th World Conference on Nondestructive Testing*, Vol. 3, pp. 1427-1433, American Society for Nondestructive Testing, Columbus, OH, 1985.

30. Reynolds, W.N., "Thermographic Methods Applied to Industrial Materials," *Canadian Journal of Physics*, 64, pp. 1150-1154, 1986.

31. Maldague, X., J.C. Krapez, P. Cielo and D. Poussart, "Inspection of Materials and Structures by Infrared Thermography: Signal Processing Techniques for Defect Enhancement and Characterization," *CSNDT Journal*, 10, No. 1, pp. 28-36, 1989.

Welcome To The:

<div style="border:1px solid">

INDUSTRIAL QUALITY, INC.

HOLOGRAPHIC & INFRARED IMAGE ANALYZER

</div>

FUNDAMENTAL STRATEGY FOR USE OF ANALYZER

VIDEO TAPE SETUP (VCR controls)
1:    Locate on the video tape the image or images to be analyzed.

SELECTING AN AREA
2:    Identify an area on the screen not more than 4 or 5 inches square which you wish to examine. The size of the area is limited by the amount of RAM available in the computer.

MAKING A BOX (F8, F9 and the UP, DOWN, LEFT, and RIGHT ARROWS)
3:    Use the arrow keys to maneuver the red dot to the top left corner of the desired area and mark it with the F8 key. Then move the dot to the bottom right corner and mark it with F9. A green box will appear. Up to 25 boxes may be drawn. Data within any of the boxes can be processed, one box at a time.

FREEZING AND UNFREEZING AN IMAGE (F5)
4:    F5 will freeze and unfreeze the image on the monitor but will not stop the video tape from continuing to run. F5 is a toggle. SHIFT F8 will freeze locally within a chosen box.

CONTRAST ENHANCEMENT OF IMAGES (CTRL F1)
5:    For manual enhancement, simply use F1, then CTRL F1, and the image on the monitor within the box will reappear with the optimum contrast possible (or as set with the ALT U function). CTRL F2 will do this automatically.

CHANGING THE UPPER INTENSITY VALUE FOR ENHANCED IMAGES (ALT U)
6:    ALT U allows the user to change the upper brightness value which the contrast enhancement function uses. (This value ranges from dark to light as it moves from 1 to 127.) The upper value simply determines whether the enhanced image will be stretched from black to the brightest value possible (127) or from black to some intermediate shade of gray (less than 127).

ELIMINATING NOISE SPIKES (ALT F3)

7: Noise spikes usually appear as one or two random points that are much brighter than all other points in the image. These very bright points will prevent an image from being contrast enhanced properly. To eliminate these points use ALT F3, enter the brightness value (1 to 127) above which the noise spikes are and below which the rest of the data is. Then press enter followed by another ALT F3. Noise spikes occur most often following the enhancement of subtracted frames.

SUBTRACTING SUCCESSIVE FRAMES (MANUAL)

8: Pause the VCR. Make a box and press F1 to save the values contained in the box into memory. Use frame advance feature to reach the desired frame and press SHIFT F1. The subtracted screen will appear on the monitor and will be stored in the RAM.

SETTING THE DELAY FOR TIME DERIVATIVE FOR AUTOMATIC SUBTRACTION

9: Two parameters are needed to define a time derivative, a delay between frames to be subtracted, and an initial delay to follow the press of the activating function key. Use the F4 and F3 keys to increase or decrease these parameters. Their current status will be printed to the screen each time F4 or F3 is pressed. Press CTRL F3 to toggle between the parameters selected for adjustment. Successive frames are 1/30 of a second apart.

TAKING THE DERIVATIVE OF FRINGE MOVEMENT (AUTOMATIC SUBTRACTION) (ALT F1)

10: This function should only be used when the tape is running at normal playing speed. At the predetermined delay after ALT F1 is pressed, the pixel values in the green box are read into memory (equivalent of an F1 operation). After the predetermined number of frames have advanced the new current image is subtracted from the image previously saved in memory (equivalent to SHIFT F1). This image is then enhanced for maximum contrast (equivalent to CTRL F1). The final image is put to the screen.

CREATING A HISTOGRAM (SHIFT F2)

11: SHIFT F2 takes whatever data is currently in the RAM (memory) and writes it to the screen in the form of a histogram. Data in the memory may not represent what is currently on the screen as not all functions update the memory when they alter the image. The data is divided into 16 groups based on the brightness of each pixel with those in group 1 being black and those in 8 being grey; each group representing a brighter distribution of points up to the 16th which is all white.

WRITING ALL DATA IN BOX TO THE DISC

12: F2 writes the brightness value and the location of all pixels within the box to a disc under a file name determined by the user.

USING MULTIPLE BOXES (F6)

13: One may create and then move among up to 25 boxes on the screen. They may be created with the F8 and F9 key. The duplication function described in section 16 will copy the box to a designated portion of the screen where the recall function will recreate a box earlier saved on the disc on the screen. At any time, one may jump through these boxes in the order in which they were created by pressing the F6 key. Each time it is

pressed you will jump to a new box. If used to jump out of the most recently created box F6 will then put the longer red dot back at the center of the screen and allow you to manually draw more boxes. F6 used again would put the red dot in the first box created. The red dot in a box signifies that this is currently the active box and all image processing functions will only affect that box.

MAKING ADDITIONAL BOXES OF EXACTLY THE SAME SIZE (SHIFT HOME, SHIFT PAGE UP, SHIFT END, SHIFT PAGE DOWN)

14: Use F6 to place the red cursor inside the box already on the screen which you wish to duplicate. To copy the box to the top right quadrant of the screen type SHIFT HOME, to the top left of the screen type SHIFT PAGE UP, to the bottom left of the screen type SHIFT END, and to the bottom right of then screen type SHIFT PAGE DOWN.

ARBITRARILY MOVING BOXES (SHIFT F7)

15: SHIFT F7 will allow arbitrary movement of a box. When SHIFT F7 is pressed, the currently selected box will disappear. Subsequent cursor motion is interpreted as motion of the center of the box. Press SHIFT F7 once again to redraw the box.

RECALLING IMAGES FROM THE DISC (SHIFT F4)

16: To recall an image that was saved earlier on the disc use SHIFT F4 and then enter the name of the file the image was saved under. You may either replace the image on the screen in the same location where it was when it was stored by entering anything except the word "HERE" to the next prompt. "HERE" tells the computer that you (and the red dot) are currently in a box with the same dimensions as the one the image was originally created in and that you wish to place the stored image in the current box.

CLEAR COLOR BOXES AND LINES FROM SCREEN AND DRAW ALIGNMENT GRID (SHIFT F5)

17: Pressing SHIFT F5 resets the number of boxes to zero and erases all past boxes and other color lines resulting from the optional red grid or the blue dots from fringe marking. This function, however, will not affect the non-colorized part of the image.

APPENDIX B

EQUIPMENT TEST PLAN

"Combined Holographic-Infrared Inspection Instrumentation"

Introduction

The research being conducted in this SBIR Phase II program will lead to the development and demonstration of a prototype combined holo-graphic-infrared inspection system for the nondestructive evaluation of composite and bonded structure. The inspection system will provide detection of discontinuities such as delaminations, disbonds, impact damage, microcracks, inclusions, etc. in honeycomb and composite struc-tures. The combined techniques provide useful diagnostic data that per-mit an inspector to determine information such as type and size of dis-continuity, depth from the surface and relative severity. The combined methods provide this information in a more complete manner than either technique used alone. Information can be obtained from the intensity and size of the indication and from the relative time for the indication to appear and dissipate. The holographic indications result from a relative movement of the stressed surface over a discontinuity, thereby pointing to a physically weak area in the structure. We have shown this to be particularly useful to detect and evaluate delaminations and disbonds relatively close to the inspected surface. The infrared results show differences in thermal properties caused by an unbonded area, microcracking, density or material property variations, etc. The two methods used together aid interpretation.

The equipment, as presently foreseen, will combine a phase-locked holograhic interferometric unit and an infrared camera into an integrated inspection system. The inspection object will be heated to excite re-sponses from each inspection mode.

This equipment test plan describes the technical characteristics of each part of the inspection system, the holographic unit and the infrared camera.

Holographic Unit

The holographic equipment will be a phase-locked holographic inter-ferometry system that will display real-time holographic interferograms through a closed-circuit television system. The holographic television system will provide 600-line resolution, 2:1 interlace composite video of real-time holographic interferograms. The initial film hologram of the inspection object will be processed in-place. Typical exposure time is 10 seconds; typical processing time 10 to 15 seconds. The holographic unit will provide capability for in-place processing, film advance, and television viewing. The holographic field of view will be at least 38 x 38cm (15 x 15 inches), as applied to a white coated (for good, uniform reflectivity) test part. The planned 35 mW HeNe laser will provide the coherent illumination. Although the phase-locked system will compensate for some movement of the monitored spot between exposures, care must be taken to support the test part to minimize movement or vibration (for ex-ample, a concrete floor, well anchored part). Care must also be provided to minimize other illumination (darkened room preferred) and temperature variations and air currents (which can change the optical path). When performed properly, the holographic unit will provide a clear and bright hologram on the video monitor, dark fringe lines when the part is stressed slightly and zero order fringes when the part is first viewed after film processing (no fringes should appear until the part is stressed).

Specifications of the planned Laser Technology Holomatic 8000 system are as follows:

Description

The Holomatic 8000 is a portable phase-locked holographic camera system for inspecting composite structures. The equipment consists of a 35 mw. HeNe CW laser, optical components, an automatic 10-second film processor, and a control unit with a built-in video monitor for viewing the holo-grams. The Laser/Camera Unit comes tripod mounted but may be detached for table top use. The holograms are made on 35mm film.

Equipment Specifications

Dimensions	Camera (Without Tripod)	Control Unit
	48 in. long	24 in. long
	11 1/4 in. high	12 in. high
	7 in. wide	10 in. wide
Power	110VAC 60Hz. 3 amps	
Laser	35 mW HeNe TEM00 Mode	

Hologram

Size	1.065 in. dia.
Processing Time	10-15 seconds, automatic
Video Monitor	9-inch (diag) 600 lines min. with BNC Connector for video recording.
Typical Target Area On Part	4 in. dia. to 18 in. dia.
Part Loading Mechanism	Thermal, Vibration, Vacuum or Pressure
BRH Classification	Class IIIB
Operating Conditions	50-110°F darkened room, no wind or apparent vibration, no thermal gradients in air path.

Infrared Camera

The infrared imaging portion of the system will provide a minimum detectable temperature variation of 0.1°C on a test part with uniform and relatively high emissivity. The spectral sensitivity range for the camera, 8 to 12 microns, will provide useful sensistivity for test parts at normal room temperature. The infrared imaging system will provide a closed circuit television image compatible with U.S. television standards; there must be interface compatibility with video recorders, the video monitor and the holographic output. The IR camera system will provide 100% line scan coverage including video line number. Some anticipated specification details of the infrared system include the following:

Field of View:	14° vertical, 18° horizontal
Spatial resolution:	1.6 mradians (50% slit contrast)
Resolvable elements per line:	250 (limiting)
Horizontal scan:	8 kHz
Active TV lines	200
Frame rate:	30Hz/2:1 interlace
Digitized signal:	256 digital samples per line; 8-bit (256) intensity levels
Frame averaging:	2 to 8 frames

Electro-optical zoom: 4:1

Detector coolant and
        hold time: Liquid nitrogen/>2hrs.

Power requirements: 12V battery or 110VAC, 60HZ

IR scanner size: 5 inch high x 4 1/4 inch wide x
                               6 1/4 inch long

IR scanner weight: 4 lbs.

Combined Inspection System

The combined inspection system will consist of a phase-locked holographic unit and an infrared camera mounted on a tripod in an arrangement as diagrammed in Figure B-1. The lens on the infrared camera can be focussed so that both inspection systems view the same area on the inspection object. The inspection object will be thermally excited by a heat gun, lamp, contact heater or other suitable thermal source for viewing by each inspection system. In addition to this combined viewing, the inspection system will also be able to provide infrared images by by through-transmission and of holographic results by other suitable excitation means (such as vibration, vacuum, or pressure). This variation in inspection object excitation will permit total flexibility with the inspection equipment. However, the prototype system will include only means for thermal excitation.

The tests for the combined system will primarily involve application of thermal energy to the inspection sample and inspection from the same side. However, as indicated, additional tests for samples, where appropriate, will be accomplished by heating the back side (through-transmission infrared) and by using other excitation methods for holographic testing.

Each inspection unit will present a television image for interpretation. At present, each system will provide such images independently. However, one of the development features that will be pursued during the Phase II program will be a possible combined television image for the two inspections. Present thinking about the dual image presentation is that the image for each technique will be optimized manually (by freezing the appropriate frame). The two images will then be combined so that the operator will be able to compare infrared and holographic results directly.

The major test for the inspection system will be the capability to image known defects in a typical aerospace component. A standardized test part that will be used to demonstrate defect capability is a graphite-epoxy skin, aluminum honeycomb core part containing known defects, as illustrated in Fig. B-2. This 1-foot-square standard is manufactured

COMBINED HOLOGRAPHIC – INFRARED INSPECTION SYSTEM
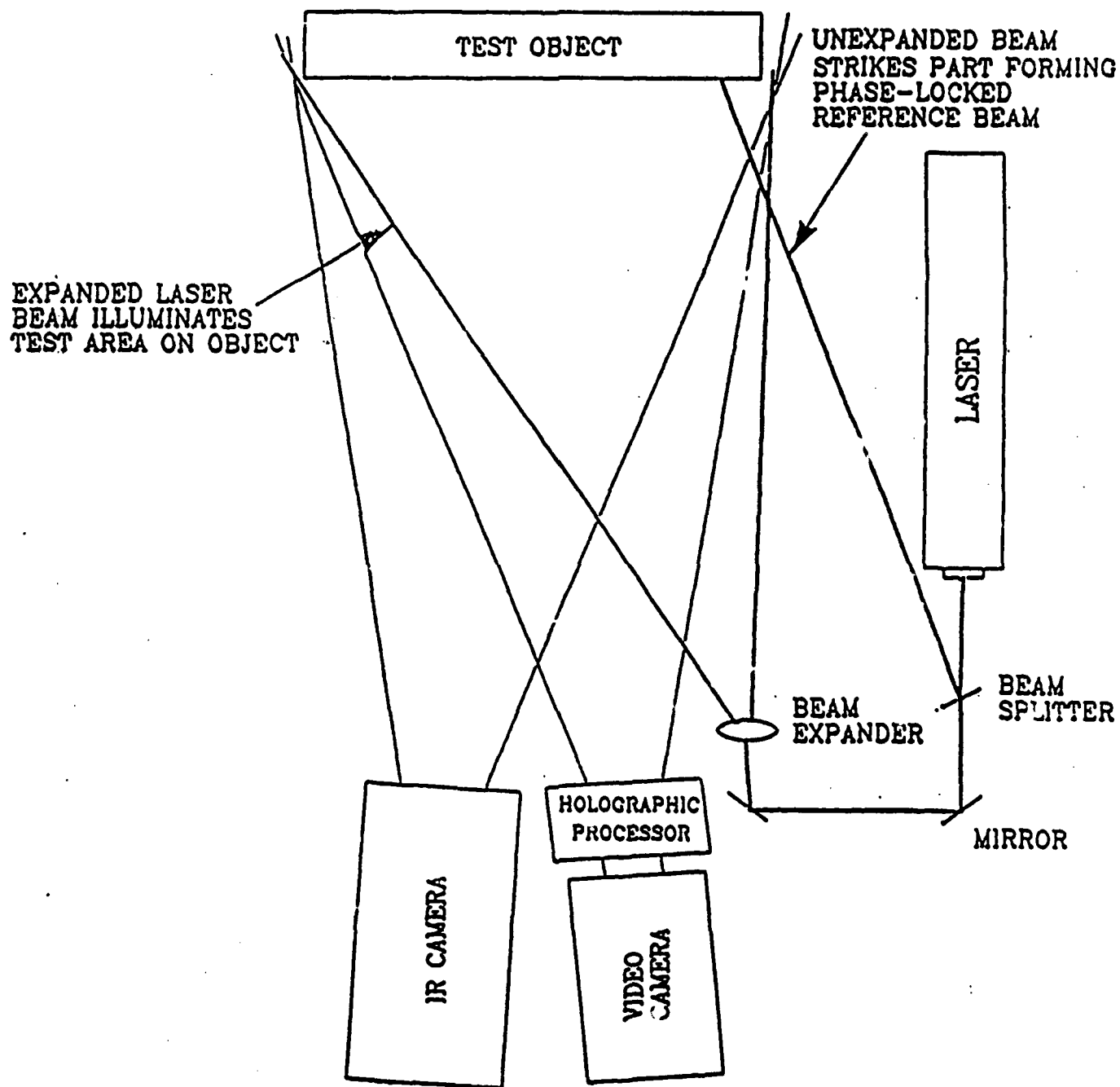
Figure B-1. Arrangement of components for combined inspection system.

DELAMINATIONS

CORE UNBONDS

EXCESSIVE ADHESIVE

CRUSHED CORE

P–1

P–2

DEFECTS SIDE
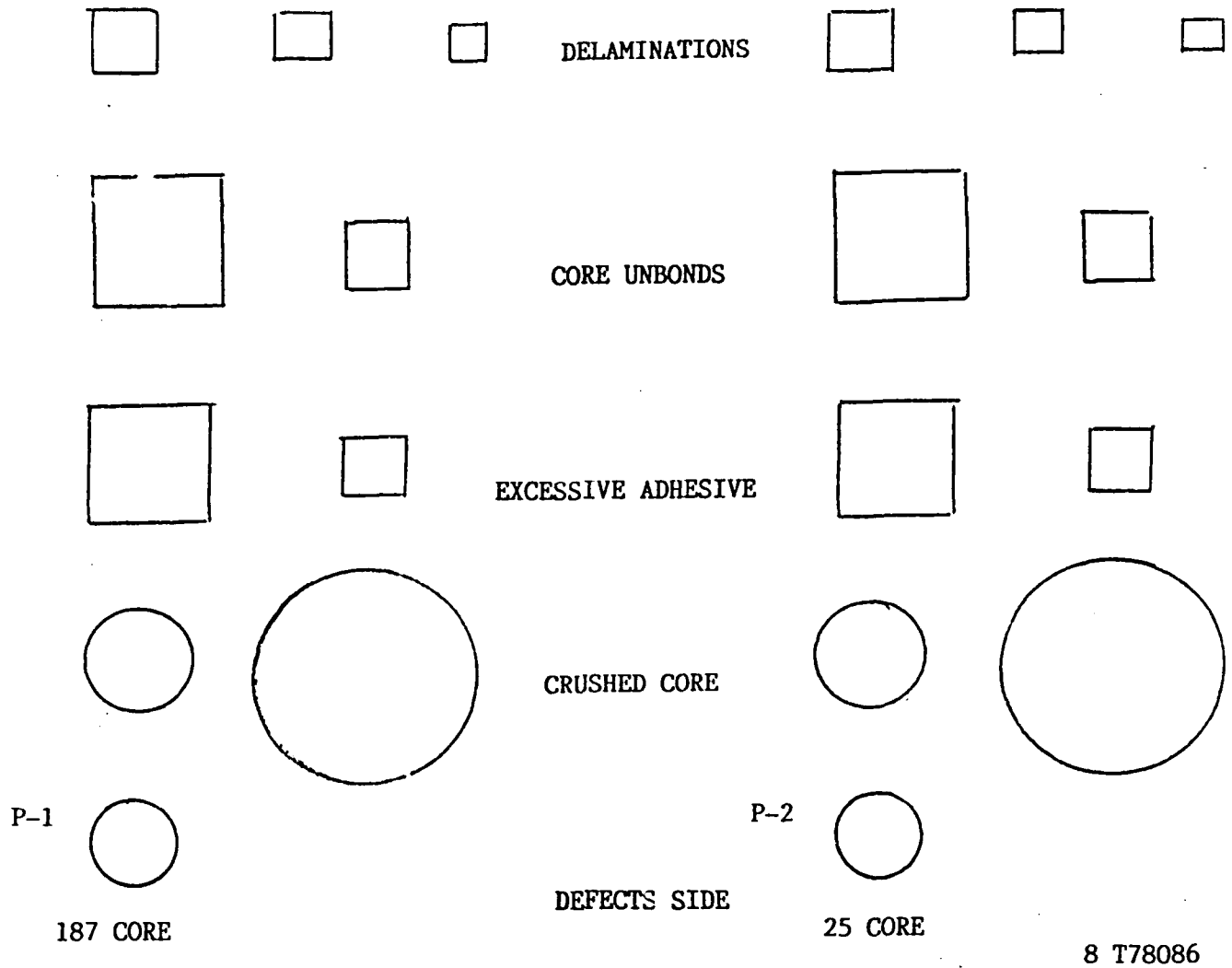
187 CORE

25 CORE

8 T78086

Figure B–2. Diagram of McDonnell Douglas NDI honeycob standard.
The smallest delamination (upper row) is 1/4 inch
square.

by McDonnell Douglas for government use for the F18 aircraft. The holographic unit will provide detection of all 1/2-inch or larger defects (except excessive adhesive; this extra adhesive will likely keep the surface skin tightly bound). The infrared unit will provide detection of all defects, including the 1/4-inch delaminations.

The nondestructive test standard is completely described in Fig. B-3. The part contains teflon inserts in the graphite-epoxy skin (total thickness, 5 plies). The inserts are placed three plies below the surface. There are also teflon inserts placed between the skin adhesive layer and the core. The part contains two different honeycomb structures, 2.3 pounds/cubic ft. (1/4-inch cells) and 3.1 pounds/cubic ft. (3/16-inch cells). The crushed core indications were placed below the skin and adhesive layers. The sizes of the indications are 1 and 1-1/2 inch diameters for the crushed core; square indications of 0.5 x 0.5 inch and 1 x 1 inch size   the extra adhesive (FM404) located below the upper skin and for the teflon inserts between the skin adhesive and the core; and square areas of teflon inserts delaminations) in the upper skin having sizes of 0.25 x 0.25 inch, 0.375 x 0.375 inch and 0.5 x 0.5 inch.

This sample is emphasized only because it has some status as a standard. However, the test plan will also involve the examination of many other inspection samples made up of various materials, thicknesses, defect types, and defect locations. Such tests will be a necessary part of the Phase II program in order to determine and demonstrate the advantages and limitations of each individual test method and the combined methods. All the test samples are not now clearly identified but the samples will include several types, such as honeycomb assemblies, solid laminates, and foam assemblies. Table B-I describes the test samples used in the Phase I program; it is planned that these samples (or similar ones) will also be available for this Phase II program. We will be alert to the availablity of inspection samples throughout the program and encourage WPAFB to assist in locating appropriate samples. We expect to test 12 samples as a minimum. Ultrasonic tests on inspection samples, for comparison, are planned.
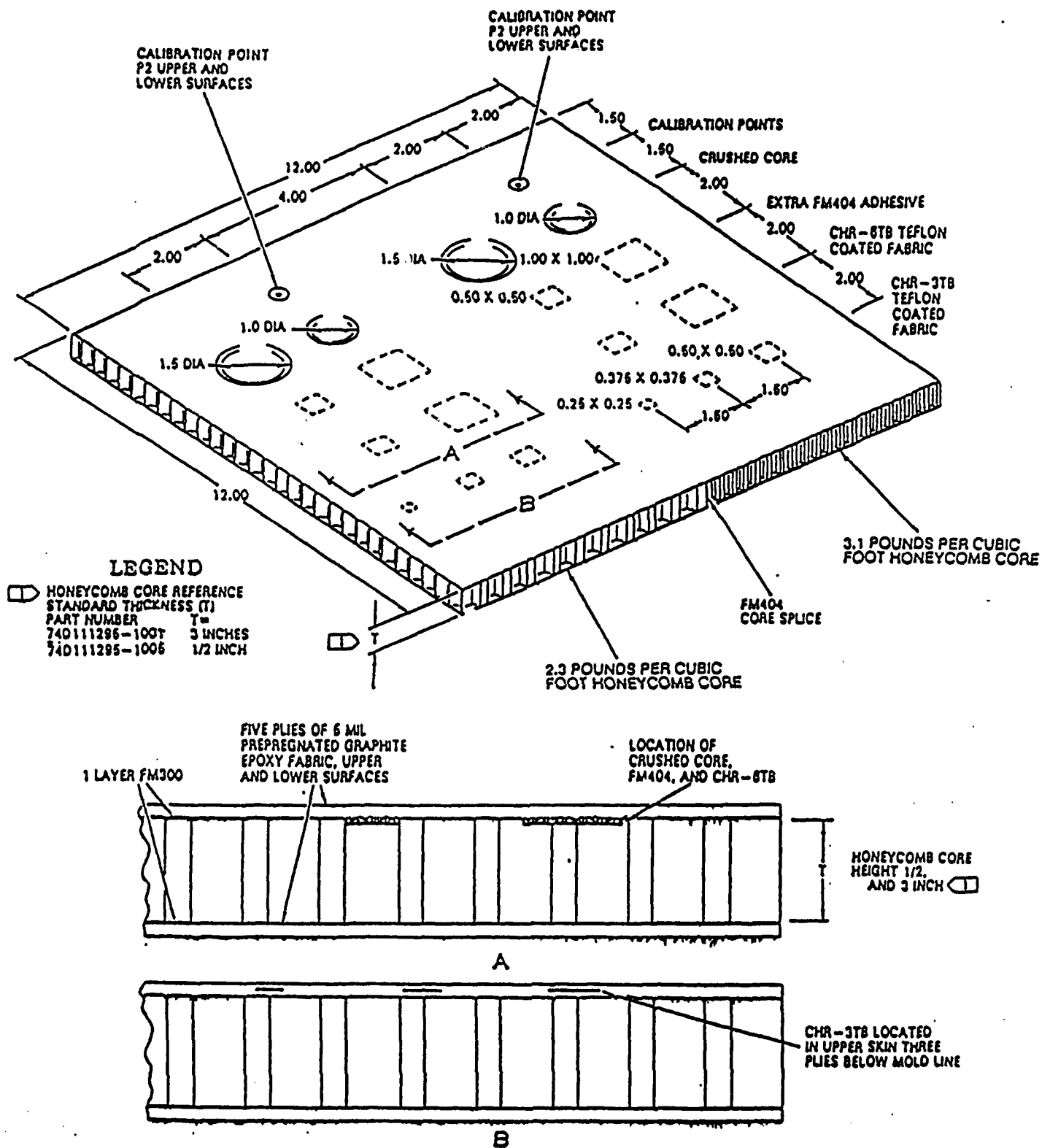
Figure B-3. Graphite Epoxy Skinned Honeycomb Core Reference Standard

TABLE B-I.   DESCRIPTION OF ADDITIONAL TEST SAMPLES

Sample No	Description
1.	Honeycomb sample, fiberglass skin, aluminum core; approximately 22 1/4 x 10 3/4 x 2 1/2 inch (58 x 27 x 6.4 cm). Graphoil, triangular inserts at various depths in the fiberglass skin.
2.	Composite sample, approximately 8 x 12 x 5/8 inch (20 x 30 x 1.6 cm). Kevlar skin/Foam Rohrcell/ Graphite skin construction. Graphoil inserts used to prepare pattern of defects.
3.	Graphite Epoxy composite, approximately 12 x 12 x 3/8 inch (30 x 30 x 0.95 cm). Impact damaged (4 through holes).
4.	Graphite Epoxy composite, approximately 12 1/2 x 1 x 1/8 inch (31.8 x 2.5 x 0.32 cm; tensile test specimen). Teflon insert.
5.	Graphite Epoxy composite, approximately 11 1/8 x 1 3/8 x 1/8 inch (28.3 x 3.5 x 0.32 cm); 17 ply. Impact damaged (ball hammer strikes) over flexible and rigid surfaces.
6.	Graphite Epoxy composite, approximately 11 x 11x1/8 inch (28 x 28 x 0.32 cm); 17 ply, 0-90 degrees. Contains naturally occurring defects.
7.	Composite sample, approximately 11 1/2 x 15 x 1 inch (29.2 x 38 x 2.5 cm). Kevlar skin/Foam Rohrcell/ Kevlar/Foam Raw Cell/Graphite skin construction. Sample contains natural defects.

APPENDIX C

Safety Assessment Report

There are only a few safety precautions to be followed in the operation of the Combined Holographic-Infrared Inspection Instrumentation. The major potential hazard to be avoided is possible eye damage from direct observation of the unexpanded laser beam in the holographic part of the equipment. The red laser light is readily visible. Operators quickly become accustomed to looking at the reflected visible light to locate objects for inspection.

The specifications for the phase-locked holographic unit incorporated in the combined system are reproduced from the Equipment Test Plan in Table C-1. The Holomatic 8000 unit, manufactured by Laser Technology, Inc., Norristown, PA, includes a 35mW Helium-Neon laser. This is classified as a Class IIIB laser. Operation of this medium output laser does not require an interlocked operation room. However, operation does require restricted access during use. The primary danger would be eye damage. Operators should be instructed to avoid looking directly into the unit while the laser is on. Also, highly reflective objects should not be placed in the path of the laser.

Under normal operating conditions, this restriction is straightforward to follow. The Holomatic 8000 unit is normally directed toward the inspection object at an operating distance of one to several feet. There is no reason for the operator to turn towards the laser when placing objects for inspection.

The developmental work on this program also demonstrated that the combined inspection system could employ an electronic shearography unit in place of the holography system. The present plan is to combine a commercial system with a Laser Technology Model ES-9100 Electronic Shearography System. That unit also includes a 35mW Class IIIB Helium-Neon Laser. Therefore, the same precautions as indicated for the Phase-Locked Holography unit apply in this case.

The only other safety issue involves the use of liquid nitrogen to cool the infrared detector. During operation, the liquid nitrogen should be replenished at about 2-hour intervals. Precautions should be taken to avoid direct contact of the skin to cold liquid nitrogen.

With these precautions in mind, an operator should experience no safety problems in the use of the Combined Holographic-Infrared Inspection Instrumentation.

TABLE C-1

The Phase-Locked Holography Unit

The Holomatic 8000 is a portable phase-locked holographic camera system for inspecting composite structures. The equipment consists of a 35-mW HeNe CW laser, optical components, an automatic 10-second film processor, and a control unit with a built-in video monitor for viewing the holograms. The Laser/Camera Unit comes tripod mounted but may be detached for table top use. The holograms are made on 35mm film.

Equipment Specifications

Dimensions	Camera (Without Tripod)	Control Unit
	48 in. long	24 in. long
	11 1/4 in. high	12 in. high
	7 in. wide	10 in. wide
Power	110VAC 60Hz 3 amps	
Laser	35-mW HeNe TEMOO Mode	

Hologram

Size	1.065 in. dia.
Processing Time	10-15 seconds, automatic
Video Monitor	9-inch (diag.) 600 lines min. with BNC Connector for video recording
Typical Target Area On Part	4 in. dia. to 18 in. dia.
Part Loading Mechanism	Thermal, Vibration, Vacuum, or Pressure
BRH Classification	Class IIIB
Operating Condistions	50-110°F darkened room, no wind or apparent vibration, no thermal gradients in air path.